Journal of Organometallic Chemistry 865 (2018) 114–127

Contents lists available at ScienceDirect

Journal of Organometallic Chemistry

journal homepage: www.elsevier.com/locate/jorganchem

Description of an unusual hydrogen bond between carborane and a phenyl group

Wenli Zou [a, c], Xiaolei Zhang [b], Humin Dai [b], Hong Yan [b, *], Dieter Cremer [a], Elfi Kraka [a, **]

[a] Computational and Theoretical Chemistry Group (CATCO), Department of Chemistry, Southern Methodist University, 3215 Daniel Ave, Dallas, TX, 75275-0314, USA
[b] State Key Laboratory of Coordination Chemistry, School of Chemistry and Chemical Engineering, Nanjing University, Nanjing, Jiangsu, 210093, China
[c] Institute of Modern Physics, Northwest University, Xi'an, Shaanxi, 710127, China

ARTICLE INFO

Article history:
Received 28 December 2017
Received in revised form
9 February 2018
Accepted 12 February 2018
Available online 16 February 2018

Keywords:
B-H…π H-Bond
Synthesis of Ir-Phosphine complexes
Borane-benzene complexes
Local stretching force constants
Bond strength orders
Energy density H(**r**)

ABSTRACT

Boranes and carboranes form non-classical H-bonds with the π-face of an arene provided entropic factors are excluded, for example via a suitably designed template. The self-assembled Ir-dithiolene phosphine complexes of the type $[Cp^*Ir(PR_3)S_2C_2B_{10}H_{10}]$ (R = C_6H_4X, X = H, F, OMe) provide such a template. Steric crowding causes that one of the B-H bonds of the carborane is positioned above the phenyl plane of R to form a non-classical B-H…π hydrogen bond. For the gas phase, this is predicted by quantum chemical calculations of the local B-H…π stretching force constants. The solid-state structures of six $[Cp^*Ir(PR_3)S_2C_2B_{10}H_{10}]$ complexes synthesized are in close agreement with the quantum chemical predictions thus suggesting the existence of B-H…π hydrogen bonds. The $^1H[^{11}B]$ NMR titration experiments reveal that non-covalent B-H…π bonds also exists in solution. Calculations show that the bond strength order of the B-H…π H-bond determined with the help of the local stretching force constant is 0.35, comparable to what is found for the H-bond in the water dimer. However, the B-H…π H-bond is electrostatic in nature as confirmed by the topological analysis of the electron density ρ(**r**). The role of this H-bond in carborane supramolecular chemistry is elucidated and discussed.

1. Introduction

Non-classical hydrogen bonds (H-bonds) between X-H donors and the π-face of an aromatic ring (X-H…π, X = C, N, O) play an important role in many biological systems [1,2] including the recognition of small organic molecules by proteins, which is a key feature in structure based drug design [3]. Although experimental and computational studies of C-H…π [4,5], N-H…π [6,7], or O-H…π interactions [8,9] in benzene-haloalkane, benzene-ammonia and benzene-water complexes have shown that these interactions are abundant and potentially important, with binding energies ΔE up to 5 kcal/mol, their nature and role is not fully understood yet.

Recently, BH…π-interactions have become a specific target for this kind of non-classical H-bonding [10–15]. In view of the electropositive character of boron (Allred-Rochow electronegativity scale [16]: χ(B) = 2.04 vs χ(H) = 2.20), B–H…π interactions should be repulsive rather than attractive unless the polarity of the B–H bond can be reversed. This is realized in boranes and/or carboranes with two-electron-three-center (2e-3c) bonding leading to a positively charged μ^2-H atom, which can be attracted by the π-density of an aromatic ring [11,13,14,17]. In particular, carboranes have drawn a lot of attention because they are structurally unique with unusual thermal, chemical and biological stabilities [18–49]. Carboranes contain both CH and BH vertexes of which the acidic C_{carb}-H bonds have been found to be H donors in classical C_{carb}-H…X (X = O, F, N, S, Cl, Br, I) [50,51] and weak non-classical C_{carb}-H…π complexes [52]. For some of the supramolecular assemblies of a carborane with a container molecule such as a calixarene or a cyclotriveratrylene [53–55] the distance between the B-H vertex and a benzene ring is in a range making attractive B-H…π interactions possible. We could verify the existence of these non-classical B–H…π interactions for the first time in a combined experimental and theoretical study on Ir-dimercapto-carborane complexes [56].

The study of B-H…π interactions is compounded because of their highly variable geometries and their sensitivity to both electronic and environmental factors. Therefore, we have carried out a

* Corresponding author.
** Corresponding author.
E-mail addresses: hyan1965@nju.edu.cn (H. Yan), ekraka@smu.edu (E. Kraka).

https://doi.org/10.1016/j.jorganchem.2018.02.014
0022-328X/

multi-pronged strategy of identifying and describing B-H…π H-bonding in detail. The current work is an in-depth extension of our previous proof of concept of non-classical B-H…π H-bonding [56] focusing on the electronic nature of such interactions and testing the usefulness of electrostatic potential, electron density and energy distribution analyses for this purpose.

The results of this investigation will be presented in the following way. First, we will describe the quantum mechanical methods we used to make reliable predictions on the existence of such non-covalent interactions (Section 2). In Section 3, we will present the computational characterization of non-classical B-H…π H-bonds. For this purpose, we will make ample use of the local mode stretching force constants of Konkoli and Cremer [57], which provide a direct measure of the strength of a given bond [58–61]. We will also determine the electrostatic and/or covalent character of bonding [62–64]. In Sections 4 and 5 we will further describe the quantum chemical and experimental verification of the non-classical B-H…π H-bond. The realization of a non-classical B-H…π H-bond will be demonstrated by a four-pronged approach involving the synthesis of the target compounds, their structural analysis via X-ray diffraction, their description in solution via ^{11}B NMR spectroscopy, and their characterization in the gas phase based on quantum chemical calculations. In this connection, we will outline pitfalls and deficiencies of approaches and techniques that are generally available and often used to describe chemical bonding. We will also address some concerns about our approach, which were recently raised in other work on BH…π interactions. (Section 4). In the last section, the conclusions of this work are summarized.

2. Computational methods

Relative energies ΔE, equilibrium geometries r_e, and normal mode frequencies ω_e of all molecules investigated in this work were determined using Density Functional Theory (DFT) with the dispersion corrected range-separated hybrid functional ωB97X-D [65,66], results of which are known to come close to Coupled Cluster results of the CCSD(T) type (CC with all single (S) and double (D) excitations, and a perturbative treatment of all triple (T) excitations) [67,68]. The def2-TZVPP basis set with the small-core ECP (effective core potential) [69] was used for Ir whereas for the other atoms the 6–31++G(d,p) basis set of Pople was employed that includes diffuse functions for both H atoms and heavy atoms [70,71]. In all cases, an ultrafine grid [72] and tight convergence criteria were used to guarantee reliable values for Hessian, vibrational frequencies, and force constants. Because of the size of most of the transition metal complexes, calculations with more than 1000 basis functions had to be performed. The two most expensive calculations included 2388 basis functions each.

The binding energies ΔE of dimers were corrected for the BSSE (basis set superposition error) utilizing the counterpoise method of Boys and Bernardi [73]. Enthalpy differences at T = 298 K, ΔH(298), and free binding energies ΔG(298) were calculated carrying out a thermochemical analysis involving zero-point energies, translational, rotational, and vibrational energy corrections as well as entropy corrections.

For all molecules investigated, natural population analysis (NPA) charges determined via a natural bond orbital (NBO) analysis [74,75] were used to quantitatively describe charge transfer and charge polarization between the monomers. The electrostatic potential (ESP) was determined and plotted for a van der Waals isosurface with a constant electron density ρ(**r**) of 0.001 atomic units (a.u.) as proposed by Bader et al. [76] in order to identify regions of positive (electrons repelling) and negative (electrons attracting) values. In several cases, results were visualized in terms of contour line diagrams using contour levels, which were defined by the formula $\pm 0.001 \times 2^n$ a.u. where the maximum n values max(n) were determined by scanning calculated ESP values.

Apart from this, a topological analysis of the electron density distribution ρ(**r**) was performed according to Bader [77]. The nature of the BH…π-interactions was determined with the help of the energy density H(**r**) calculated at the (3,-1) bond critical point $\mathbf{r}_b$ of the electron density distribution. We applied the Cremer-Kraka criteria of covalent bonding [62–64]: i) A zero-flux surface and bond critical point $\mathbf{r}_b$ has to exist between the atoms in question (necessary condition) and ii) The local energy density at H($\mathbf{r}_b$) must be negative and thereby stabilizing (sufficient condition for covalent bonding). A positive H($\mathbf{r}_b$) indicates a dominance of electrostatic interactions [62–64]. In this way, it was clarified whether BH…π-interactions are weakly covalent, electrostatic, or a mixture of both.

Local vibrational modes were derived from the calculated normal vibrational modes using the Konkoli-Cremer method [57]. This is based on solving the mass-decoupled analogue of the Wilson equation of vibrational spectroscopy [78]. In this way, kinematic (mass) coupling is eliminated and local (uncoupled) modes are obtained as has been demonstrated by Cremer and co-workers [58,59,79–82]. The local stretching force constant k_a(AB) of a bond AB is the perfect measure for its intrinsic strength [61,83–85]. This does not hold for the local stretching frequency ω_a, which depends also on the masses of atoms A and B thus disguising the electronic origin of the bond strength [58–61].

In the case of dimers such as BH_3…benzene, there are six local intermonomer vibrations that can be described by determining the center of mass for each monomer and then obtaining the corresponding local stretching, bending, and torsion modes [86]. For example, the local intermonomer stretching vibration between one atom of the first monomer (H atom of a B-H bond) and the center of mass of the second monomer can be uniquely determined utilizing the approach by Konkoli and Cremer [57]. In the case of an asymmetrically positioned BH group, the projection of the H atom onto the ring plane should be used rather than the center of mass. A caveat is appropriate; calculating first the individual BH…C interactions and then averaging over these interactions leads to the wrong description, as the number of local modes must be equal to the number of normal modes, If, e.g., in the case of BH_3…benzene, the average of the six local (B)-H…C stretching force constants is used, pseudo-bending and pseudo-torsional modes are erroneously introduced that do not correspond to the correct local intermonomer bending and torsion modes. In this way, the value of the local BH_3…benzene stretching force constant will be largely underestimated and does no longer describe the BH…π H-bond correctly. If defined correctly as done in this work, the local intermonomer stretching force constant is a quantitative measure of the intrinsic strength of the BH…π-interaction.

In the case of a transition state (TS), an additional translational mode has to be projected out of the set of 3 N - L (L = 5 or 6) normal modes thus leading to 3 N - (L + 1) vibrational modes, for which the Konkoli-Cremer formalism [57] can be applied in the same way as for a molecule at equilibrium. There is a one to one relationship between normal and local vibrational modes, which can be verified with an adiabatic connection scheme (ACS) [58,79]. In the case of a monomer consisting of a transition metal and ligands that have an additional through-space interaction, the deformation mode of the cyclic system formed via H-bonding with the largest BH…π stretching contribution is converted into a local BH…π stretching mode thus limiting the number of local modes to 3 N - L.

When comparing a large set of local stretching force constants k_a, the use of a relative bond strength order (BSO) n is convenient [61,82,85]. Relative BSO values n are obtained by utilizing the

extended Badger rule [61,82,87,88], according to which n is related to the local stretching force constant by a power relationship. This is fully determined by two reference values and the requirement that for a zero-force constant n becomes zero. In the current work, we used as reference bonds the F-H single bond (n = 1.0) and the delocalized $[F\ldots H\ldots F]^-$ bond (n = 0.5) to obtain the explicit form of relationship (1)

$$n = a(k_a)^b \quad (1)$$

The parameters a and b, (a = 0.6768 and b = 0.2908) were determined with the help of the k_a values calculated with the method and basis set described above for the two reference bonds. To simplify the analysis, the BSO values n obtained in this way were adjusted to the standard n(B-H) = 1.000 by using the local stretching force constant of the B-H single bond in BH_3 as scale factor.

All vibrational mode, BSO, and electron (energy) density calculations were carried out with the program package COLOGNE2016 [89], whereas for the DFT calculations Gaussian09 [90] was used. The ESP analysis and electron density topological analysis [77] were carried out with MultiWFN [91], while the Symmetry-Adapted Perturbation Theory (SAPT) [92,93] and the Localized Molecular Orbital Energy Decomposition Analysis (LMOEDA) [94] were performed with PSI4 [95] and GAMESS [96], respectively.

3. Quantum chemical prediction of a non-classical H-bond of the B-H…π type

In Fig. 1, B-H containing molecules and dimers are presented, where the latter might be characterized by a B-H…π H-bond. Because of the electronegativity difference between B and H ($\Delta\chi = \chi(H) - \chi(B) = 0.19$, Allred-Rochow scale [16]), the H atoms in BH_3 (**R1**) are negatively charged (−0.10 e, Fig. 1). If **R1** approaches benzene so that one of its BH bonds is forced to be perpendicular to the ring plane and oriented along the C_6-axis, a second order transition state (TS(2nd)) of the PES is obtained (**R2**) at a H-ring distance d of 2.705 Å (d is always the shortest distance between H and the plane of the benzene ring). The binding energy ΔE is −1.33 kcal/mol at this point. The equilibrium form **R3** of the complex BH_3-benzene is obtained after an internal rotation of **R1** into a plane (almost) parallel to the benzene plane (ΔE: −3.04 kcal/mol). In this way, the B atom with its pπ-hole gets close to an occupied C-π-orbital; (B-C distance: 2.850 Å). Hence, **R1** prefers a stacked arrangement of the monomers, which is in line with the early results of Tarakeshwar and co-workers [10].

In **R3**, there is a charge transfer of 64 me (milli-electron) from the benzene ring to the BH_3 molecule, which, besides electrostatic interactions, contributes to the stability of the dimer. Similar results for **R3** were recently reported by Grabowski [97]. The charge transfer is facilitated by a slight polarization of the benzene molecule from C8 (in *p*-position to the B…C interaction) to C5 (involved in the interaction, see Fig. 1). The negatively charged H atoms H3 and H4 are positioned above and between the positively charged benzene atoms H16 (2.99 Å), H11 (2.85 Å), and H12 while H2 of BH_3 is placed above the density minimum close to the center of benzene. This facilitates the electrostatic attraction between the two monomers. For the 2nd order TS **R2**, the stability results from a mutual polarization of the monomers. The charge transfer from benzene to BH_3 (4 me) is small. We note that complex **R3** does not contain any stabilizing B-H…π interactions and can only be observed at low temperatures. At room temperature, **R3** is entropically destabilized as reflected by a ΔG(298) value of 4.9 kcal/mol (Fig. 1).

One might argue that B-H…benzene H-bonding can be enforced by reducing the charge at H(B). Electronegative substituents such as F atoms as in HBF_2 (**R4**) might lead to a H-bonded benzene complex. However, complexes such as **R5** (again a TS(2nd)) and **R6** are even less stable than **R2** and **R3,** although the positive charge at B is increased from 310 me to 1150 me. This is a result of charge alternation, which increases the negative charge at H (−140 me; Fig. 1) and by this the repulsion between the benzene ring and HBF_2. Noteworthy is that the local B-ring stretching force constant of **R6** (0.131 mdyn/Å) is significantly larger than that of **R3** (0.089 mdyn/Å) indicating that the larger charges at B, F, and H lead to a larger electrostatic attraction with the ring.

The results summarized in Fig. 1 reveal that H-bonding involving a conventional B-H bond as a donor and the π-cloud of an aromatic system as an acceptor is energetically not favorable. However, possible is a charge-transfer complex between the electron-deficient diborane **R7** and benzene, provided that one of the positively charged H atoms is placed above the center of the benzene ring [11–14]. In Fig. 1, a C_{2v}- and a C_s-symmetrical donor-acceptor complex, **R8** and **R9** (the BB axis is parallel and rotated by 30° relative to the 1,4-CC-axis of benzene) are shown, which have binding energies ΔE of −4.7 and −5.1 kcal/mol. **R8** is a first order TS for a rotation of B_2H_6 at the C_2-axis of the complex (another TS is found when the BB axis and the 1,4-CC axis are perpendicular), which leads to the equilibrium form **R9**. Again, there is a small charge transfer from the ring to the B_2H_6 molecule (−15 me in both cases) and the bonding is predominantly electrostatic (H5 above benzene: +130 me). The distance values d between H8 and the ring are 2.496 and 2.483 Å for **R8** and **R9**, respectively. The corresponding intermonomer stretching force constants are 0.126 and 0.086 mdyn/Å. Hence, one can speak of H-bonding although this is of electrostatic nature in view of the small charge transfer and positive (destabilizing) energy densities $H(\mathbf{r}_b)$ [62–64] at the critical points between the ring and H8 (see Table 1).

We investigated also the interaction between *closo*-carborane **R10** with benzene. The H-bonded structure **R11** is neither a minimum nor any (higher order) TS and converts to **R12**, which is electrostatically better stabilized because of the attractions between 3 positively charged carborane H atoms and the negatively charged benzene C atoms, for the prize of experiencing also some repulsion with the positively charged benzene H-atoms. All calculated binding energies are smaller (or more positive) than in **R8** and **R9** (ΔE: −3.9, ΔH(298): −2.8, and ΔG(298): 3.5 kcal/mol, see Fig. 1). The local stretching force constant (0.059 mdyn/Å) is just one half of that in **R9**.

Stable complexes can be obtained by orienting one of the C-H bonds of o-$C_2B_{10}H_{12}$ toward the face of a benzene ring (see **R13** in Fig. 1). Dimer **R13** has a binding energy of −7.9 kcal/mol (d = 2.361 Å, charge transfer −12 me; stretching force constant 0.095 mdyn/Å, Table 1), where the increased stability of the complex is a direct consequence of the larger positive charge at the H atom above the benzene plane (see Fig. 1).

We conclude that B-H…benzene H-bonds exist provided the interacting H is positively charged as in the case of electron-deficient polyboranes (B_2H_6, B_5H_9, $B_{10}H_{14}$ [17]) and carboranes ($C_2B_{10}H_{12}$ [17]). They should be measurable at lower T rather than at room temperature, as is suggested by the calculated ΔG(298) values in Fig. 1.

4. Verification of the non-classical B-H…π H-bond

There are two possible ways of experimentally detecting a H-bond of the B-H…π type. The first requires low temperature studies, for example with the help of matrix isolation spectroscopy or, alternatively, supersonic jet expansion studies of complexes **R9**, **R12**, or in general (carbo)borane, or arene complexes. The

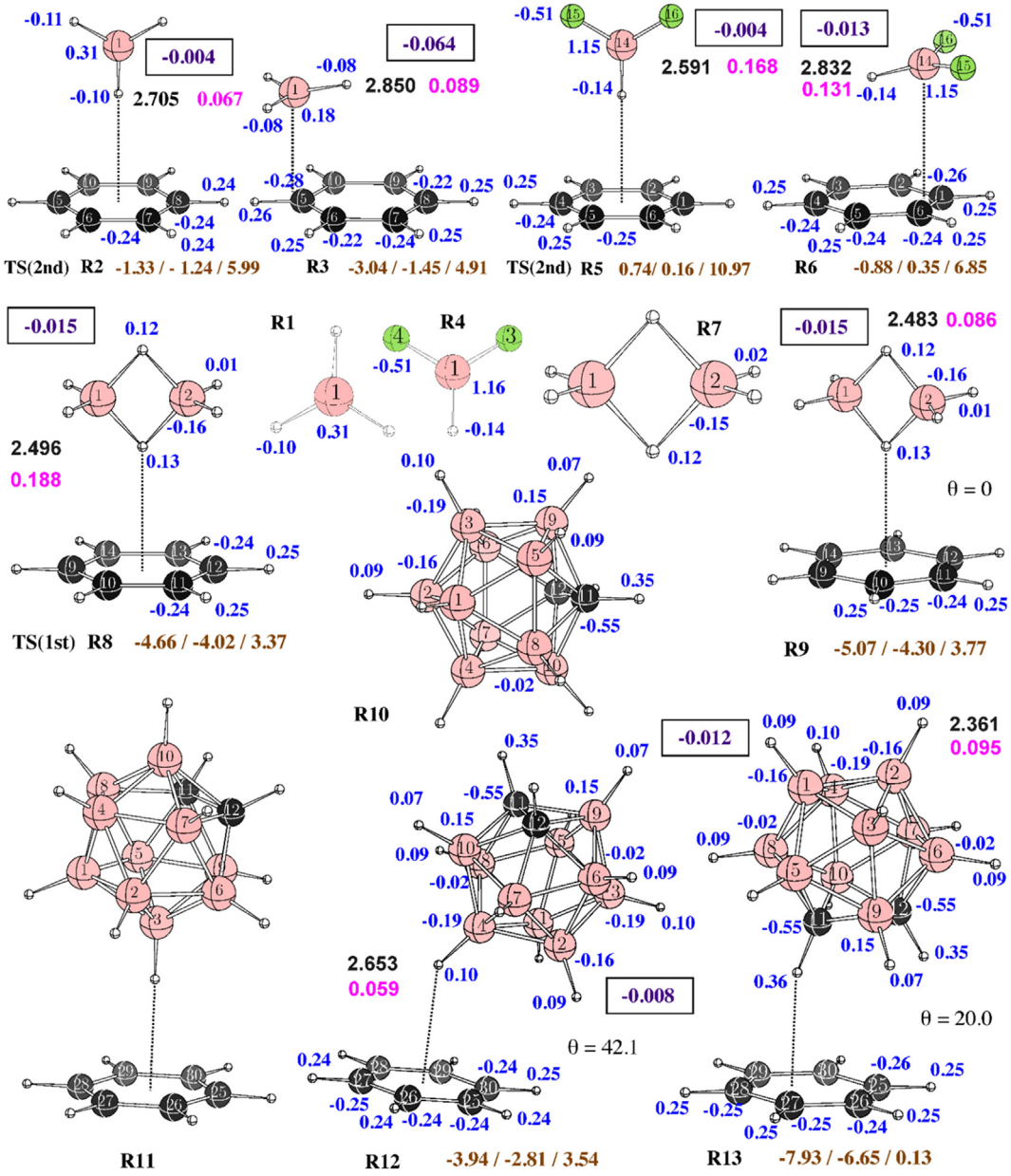

Fig. 1. Calculated properties of reference molecules **R1** - **R13**. Binding energies (in kcal/mol) in bold brown numbers separated by slashes: first value: ΔE; second value: ΔH(298); third value: ΔG(298); bold black numbers: distance d between BH-hydrogen and benzene plane in Å; purple numbers: (B-)H…benzene stretching force constants in mdyn/Å; numbers in boxes: total charge transfer from benzene to the borane or carboborane in electrons; blue numbers close to atom balls: NPA charges of symmetry-unique atoms. Transition states (TS) of first order (1st) and second order (2nd) are indicated. ωB97X-D/def2-TZVPP, 6−31++G(d,p) calculations. (For interpretation of the references to color in this figure legend, the reader is referred to the Web version of this article.)

generation of the interacting monomers would be a challenge and, therefore was not pursued in this work. Alternatively, one could stabilize a BH…π interaction by incorporating it into a suitable template that places a polar B-H bond in the vicinity of a benzene ring, as shown in Fig. 2 (situations I and II). Situation I would correspond to a normal BH ($B^{\delta+}$- $H^{\delta-}$) bond that attracts two partially positively charged H atoms of a benzene molecule in the sense of a dihydrogen interaction. In this work, we were interested in situation II and the experimental realization of a B-H…π H-bond, which implies that any C-H…π interactions are replaced by the corresponding B-H interactions as shown in Fig. 2.

A suitable template can be built by starting from a half-sandwich dithiolene complex **B** of the type [$Cp^*Ir(S_2C_2B_{10}H_{10})$] (see Fig. 3) that provides BH bonds with positively charged H atoms (Fig. 4, left side). An attempt to enhance this effect in complex **C** (Fig. 4, right side) by placing two carbon atoms into positions 9 and 10, so that they form with the sulfur atoms S2 and S3 and the Ir atom a 5-membered ring that could be stronger electron-withdrawing than the corresponding five-membered ring with two B atoms in Fig. 4 (left side) was not successful as the charge reorganization takes place predominantly in the 5-membered ring but not with regard to the H atoms in o-position and being accessible to a sideward approach of an arene ligand: The charges of these H(B) atoms remain at 90 me (see Fig. 4). The positive charge of an inwardly oriented H(B) in molecule **B** is somewhat larger, but being placed below the Cp^* ligand, H(B) should not be accessible to other ligands.

Both **B** and **C** are 16-electron (16e) complexes of iridium, which

Table 1
Distances d, local stretching force constants k_a, local stretching frequencies ω_a, BSO values n, electron densities ρ_b, and energy densities H_b of B-H and B-H…π H-bonds.

Molecule	Interaction	d[a] (Å)	k_a (mdyn/Å)	ω_a (cm^{-1})	n	ρ_b[b] (a.u.)	H_b (a.u.)
R8, **TS1**	B-H	1.315	1.937	1887	0.820		
	H…X(C_6)	2.496	0.188	567	0.377	0.0067	0.0011
R9	B-H	1.315	1.672	1753	0.786		
	H…X(C_6)	2.483	0.086	382	0.300	0.0068	0.0011
R8, **TS2**[c]	B-H	1.315	1.937	1887	0.820		
	H…X(C_6)	2.500	0.175	546	0.369	0.0066	0.0011
R12	B-H	1.185	3.989	2708	1.012		
	H…X(C_6)	2.653	0.044	276	0.247	0.0057	0.0010
R13[d]	C-H	1.082	5.800	3254	1.021		
	H…X(C_6)	2.361	0.095	402	0.309	0.0092	0.0011
B1	B-H	1.180	4.104	2747	1.020		
	H…X(C_6)	2.443	0.143	495	0.348	0.0084	0.0014
B2	B-H	1.180	4.106	2748	1.021		
	H…X(C_6)	2.432	0.142	492	0.347	0.0087	0.0013
B3	B-H	1.179	4.089	2741	1.019		
	H…X(C_6)	2.422	0.159	520	0.359	0.0089	0.0013
C1	B-H	1.172	4.273	2803	1.032		
	H…X(C_6)	2.368	0.158	519	0.358	0.0098	0.0015
C2	B-H	1.173	4.277	2804	1.033		
	H…X(C_6)	2.365	0.161	524	0.360	0.0098	0.0015
C3	B-H	1.172	4.290	2808	1.034		
	H…X(C_6)	2.346	0.167	534	0.364	0.0096	0.0015
R1	B-H	1.195	3.743	2623	1.000	0.1820	−0.1939

[a] The distance d for H…X(C_6) H-bonds (X gives the projection of H in the benzene or phenyl ring plane) is defined in Fig. 9.
[b] Density at the (3,-1) critical point.
[c] TS2 (not shown in Fig. 1) corresponds to another first order TS obtained by a 90°-rotation of B_2H_6 in TS1.
[d] The BSO value n of the CH bond was obtained using an *a* value of 0.6121 in Eq. (1).

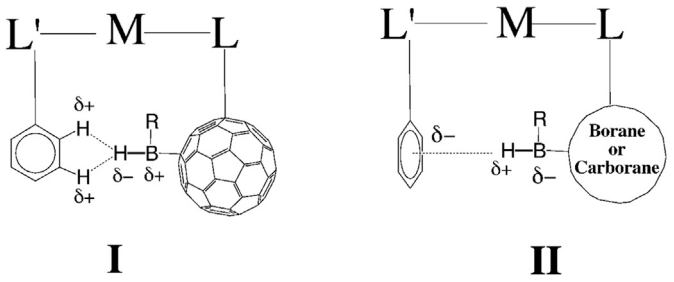

Fig. 2. Possible templates to foster the normal BH interaction with a phenyl ring (situation I) or to enforce a B-H…π H-bond. M is a transition metal with ligands L and L′ and a suitable sterically demanding linker group, which places the B-H bond in the position close to a phenyl group so that either the electronic situation I or II might results.

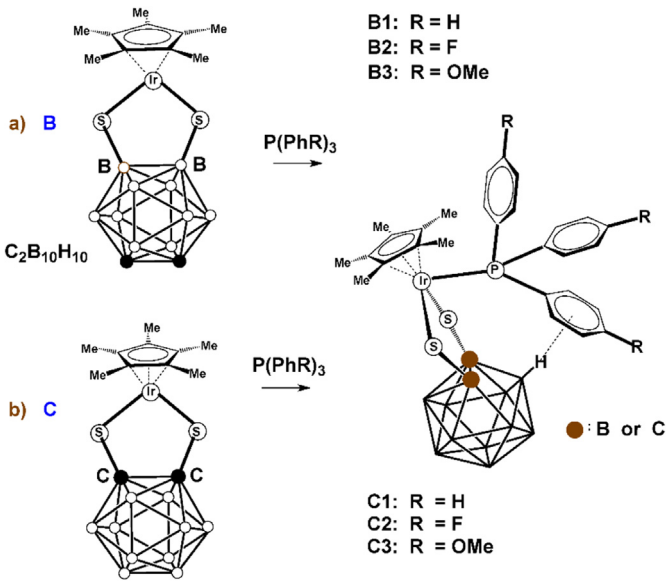

Fig. 3. Formation of a phosphine-iridium complex containing the B-H…π H-bond. Starting from the 16e complexes **B** in a) and **C** in b), 18e Ir-complexes **B1**-**B3** and **C1**-**C3** are formed.

can stabilize itself by accepting 2 electrons from an additional ligand, thus forming an 18e iridium complex. Iridium phosphine complexes are known to be stable [98]. Phosphines have the advantage of being easily tunable with regard to electronic and steric properties. Using an aryl substituted phosphine, there is a high possibility of enforcing a carboborane-aryl interacting as indicated by template II in Fig. 2.

In view of these considerations we have followed a multi-pronged approach by i) carrying out extensive quantum chemical calculations for potential target systems **Bn** and **Cn** (n = 1, 2, 3) of Fig. 3, ii) synthesizing compounds **Bn** and **Cn**, iii) determining their geometry in the solid state with the help of X-ray diffraction studies, and iv) characterizing their structure in solution utilizing NMR spectroscopy.

H(r) are shown for the carborane-benzene complexes **R12** and **R13** (bottom left and right) for the same reference plane where solid (dashed) contour lines indicate a positive (negative) energy density. The energy density diagrams, contrary to the ESP diagrams, clearly indicate non-classical (B)-H…π and (C)-H…π interactions.

4.1. Properties of the B-H…π H-bond

According to the DFT calculations, the B-H bonds close to the five-membered ring have similar polarities (B: −0.01 e; H: 0.09 e) for **B1** and **C1,** where in the first case negative charge is accumulated at the sulphur atoms, which is revealed by the calculated NPA charges (see Supporting Information in Ref. [56], denoted as SI in the following text) and the ESP shown in Fig. 5 (upper part; indicated by the red color). For **C1**, the ESP has a different form (lower part, Fig. 5) in the carborane part, caused by the incorporation of the C atoms into the 5-membered ring and a withdrawal of negative

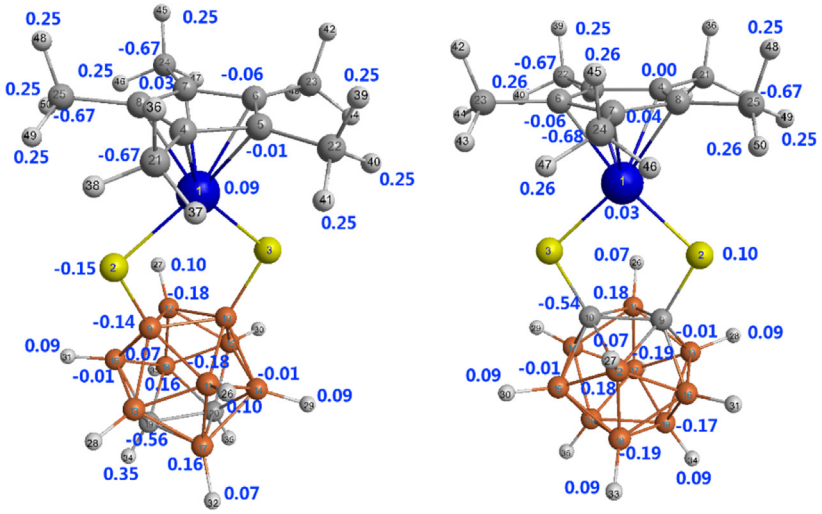

Fig. 4. Structure and charge distribution of the starting complexes **B** (left) and **C** (right). Color code: blue, iridium; yellow, sulphur; brown, boron; grey, carbon; light grey, hydrogen. NPA charges in e (blue). ωB97X-D/def2-TZVPP, 6–31++G(d,p) calculations. (For interpretation of the references to color in this figure legend, the reader is referred to the Web version of this article.)

charge from the S atoms. The ESPs for **B1** and **C1** are different especially in the region of the Ir-dithiolene unit. There might be the onset of a σ-hole [99,100] around the H(-B) atom (the light green color indicates a positive ESP) that attracts the π-density of the phenyl ring.

Closer inspection of the cleft region between phenyl group and carboborane ring as well as of the assumed σ-hole seems to exclude an electrostatic attraction between B-H bond and phenyl ring. Fig. 6 displays for both **B1** and **C1** a contour line diagram of the ESP in the plane of the BH bond and its projection onto the phenyl ring. The ESP is largely positive (solid contour lines) for this plane and does not reveal any specific interaction for **C1,** whereas for **B1** one might speculate that the BH bond as well as the phenyl ring are both attracted by a small region of negative ESP (dashed contour lines).

At this point, one has to remember that bonding (covalent and/or electrostatic) is always the result of a potential energy and a kinetic energy change, as was first convincingly demonstrated by Ruedenberg in the case of the H_2^+ and H_2 molecules [101,102]. If one exclusively focuses on the ESP (reflecting the change of the potential energy), then the kinetic energy as an important component of bonding is neglected and conclusions just drawn on the existence of a ESP-based "σ-hole" become questionable, as is demonstrated in the current case: The ESP shown in Figs. 5 and 6 does not necessarily proof the existence of a B-H…π H-bond, and the reason is obvious: The ESP is always positive around the nuclei and even in the bonding region (c.f. the B-H, C-H, and P-C bonds in Fig. 6), because in these areas the contribution from positive nuclear charge is much stronger than that from negative electronic charge. The ESP becomes only meaningful if analyzed on a molecular surface far away from the nuclei; e.g. the van der Waals isosurface with $\rho(\mathbf{r}) = 0.001$ a.u. [76]. Table 1 shows that ρ_b of the B-H…π H-bonds in **Bn** and **Cn** is about 0.009 a.u., being out of the range of $\rho(\mathbf{r}) = 0.001$ a.u.; therefore, the ESP is not suitable to analyze the B-H…π H-bonds.

A reliable indicator of covalent and/or electrostatic interactions is the energy density $H(\mathbf{r}) = G(\mathbf{r}) + V(\mathbf{r})$ originally introduced by Cremer and Kraka to distinguish between covalent and electrostatic bonding [62–64]. We have calculated $H(\mathbf{r})$ for the same plane (see Fig. 7) for which the ESP is shown in Fig. 6. The energy density $H(\mathbf{r})$ is negative for the covalent BH and other covalent bonds (indicated in this case by solid contour lines). Close to the atoms a spherical slightly perturbed shell structure is visible, which indicates the transition from core to valence region by the change from negative to positive (dashed contour lines) and then negative contour lines.

Opposite to the BH bond in the plane of the phenyl ring, there is a region of positive energy density. Electron density always accumulates in a region of negative energy density because this leads to a stabilization of a molecule, as was originally pointed out by Cremer and Kraka [62–64]. Electron density is depleted in a region of positive energy density. Therefore, it is justified to consider regions of negative energy density as electrophilic and those of positive energy density as nucleophilic areas. Accordingly, there is an electrostatic attraction between an electrophilic region and a nucleophilic region as is indicated by the (solid) contour lines extending from the H atom into the direction of the positive energy density. The interaction should be somewhat stronger in the case of **C1** as the orientation of the B-H bond is almost perpendicular to the phenyl plane and points with its H-end directly into the region of positive energy density (Fig. 7).

Similar conclusions can be drawn when comparing contour line diagrams calculated for the ESP of the carborane-benzene complexes **R12** and **R13** (top left and right of Fig. 8) with those of the corresponding contour line diagrams of the energy density $H(\mathbf{r})$ (bottom left and right of Fig. 8). In both cases, only the energy density reveals an attraction between the carborane B-H (left) or C-H bond (right side) and the benzene ring suggesting non-classical H-bonds, whereas the ESP (top of Fig. 8) is not conclusive.

We can quantify the strength of the (B)-H…π interactions in **B1** and **C1** by referring to the calculated local stretching force constants k_a involving the H(B) atom and the π-face of the ring. The values are 0.143 mdyn/Å in the case of **B1** and 0.158 mdyn/Å for **C1** that correspond to BSO values of 0.348 and 0.358, respectively (see Table 1). These values provide important information: i) The non-classical (B)-H bond has a strength that is just one third of that of a normal B-H bond (see Table 1). At the (3,-1) bond-critical point r_b, the value of ρ_b is small (<0.01 a.u.) and the energy density H_b is positive in contrast with the normal B-H bond as revealed in Table 1. Therefore, according to the Cremer-Kraka criteria, there is a dominance of electrostatic interactions [62–64]. ii) The somewhat stronger interaction is obtained for **C1** (BSO value of 0.358 vs. 0.348, Table 1), in line with the predictions based on the inspection of the energy density diagrams shown in Fig. 7. We note that this insight is

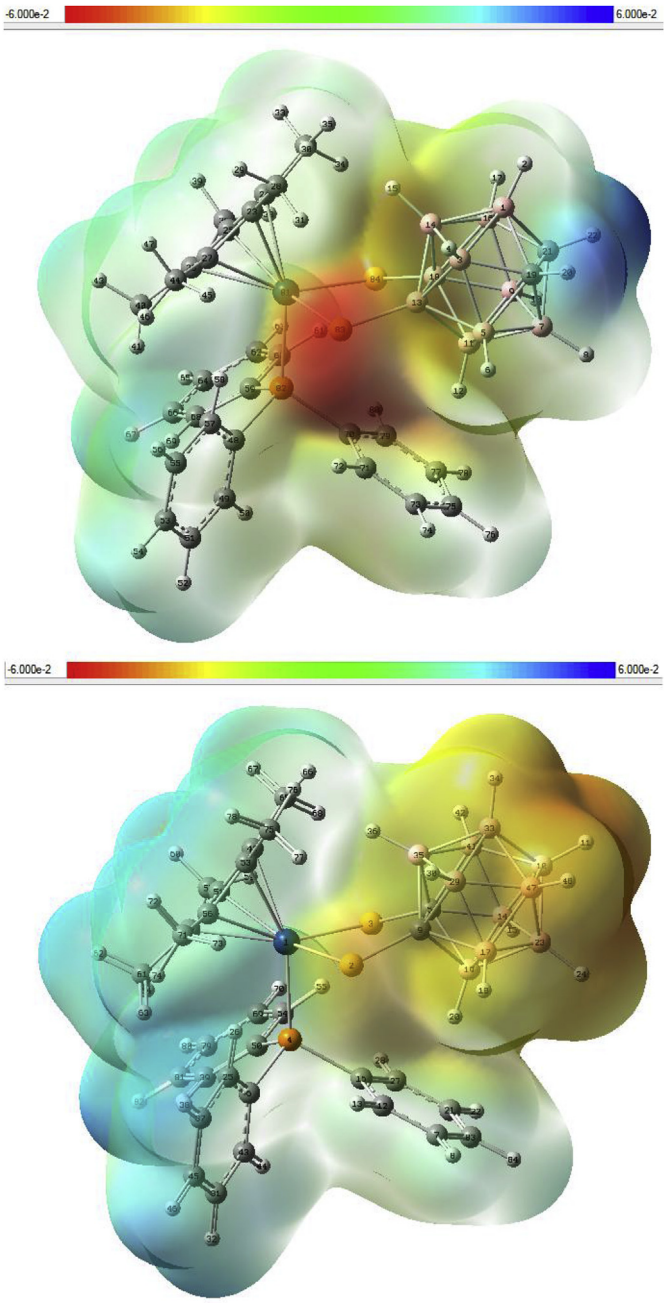

Fig. 5. Three-dimensional perspective view of the ESP of **B1** (above) and **C1** (below) calculated for an isosurface with the density of 0.001 a.u. at the ωB97X-D/def2-TZVPP, 6−31++G(d,p) level of theory utilizing optimized geometries. One of the BH bonds is pointing in the direction of a neighboring phenyl ring, which has its π-face oriented toward this B-H bond. Although the H(B) seems to be in a positive region of ESP, it is not possible to anticipate the values of ESP inside the cleft being formed by the phenyl ring and the carborane-ligand.

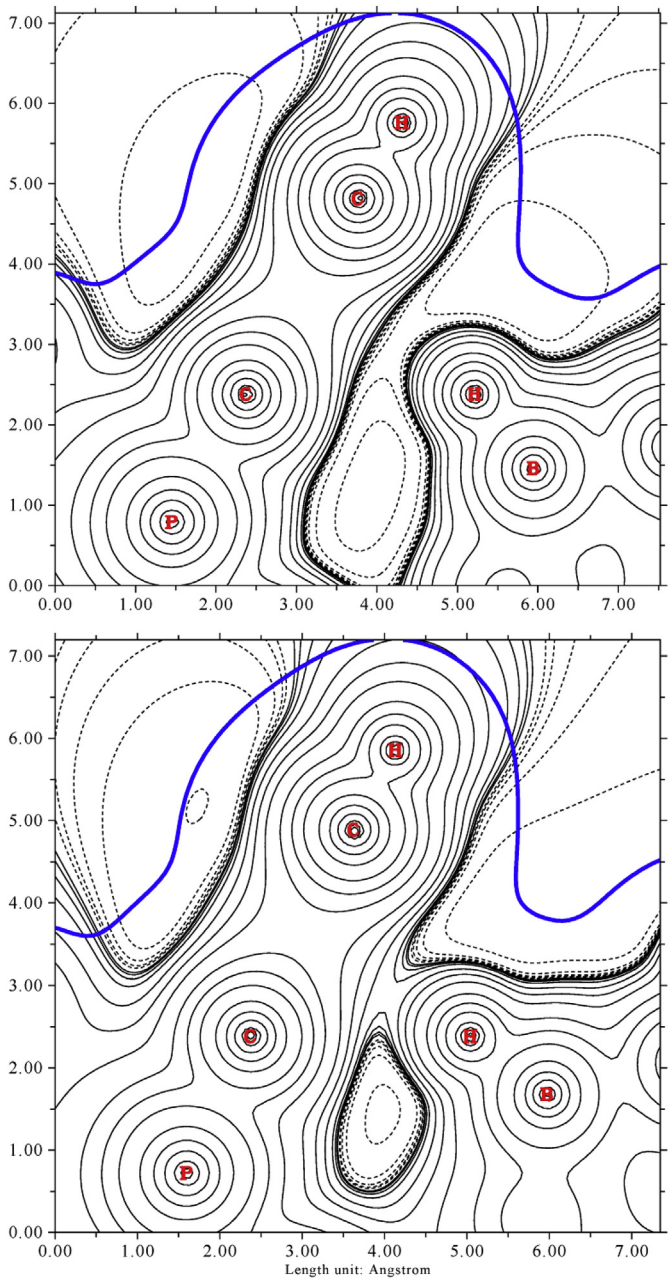

Fig. 6. Contour line diagram of ESP calculated for **B1** (top) and **C1** (bottom) in the plane defined by the BH bond and the projection point of H in the plane of the neighboring phenyl ring, that is shown in a sideward view so that only the P-C bond and the p-positioned C-H bond can be seen. Solid (dashed) contour lines correspond to a positive (negative) value of ESP, whereas the blue line is the van der Waals isosurface with ρ(r) = 0.001 a.u. (For interpretation of the references to color in this figure legend, the reader is referred to the Web version of this article.)

not provided by either the ESP shown in Fig. 5 nor the more detailed contour map of ESP in Fig. 6.

4.2. How is the B-H…π H-bond formed?

Generation of complexes **Bn** or **Cn** implies a reaction of **B** or **C** with a phosphine. If the P→Ir bond is formed, the Ir-ligand Cp* is tilted to the back thus avoiding some of the repulsive interactions with the incoming triarylphosphine ligand. The phenyl groups have to arrange in a propeller form to avoid strong destabilizing exchange repulsion. This in turn leads to the fact that one of the phenyl groups is positioned in such a way that a B-H…π H-bond becomes possible. We have verified this H-bond by optimizing the geometry of the six iridium complexes **B1**, **B2**, **B3**, **C1**, **C2**, and **C3**. Then, we have calculated NPA charges, the ESP, electron density and energy density distributions, and normal vibrational and local vibrational modes. Utilizing the latter, local stretching force constants k_a were calculated for the six different B-H…π H-bonds.

Distances d and L (see Fig. 9) are between 2.35 and 2.44 Å, no

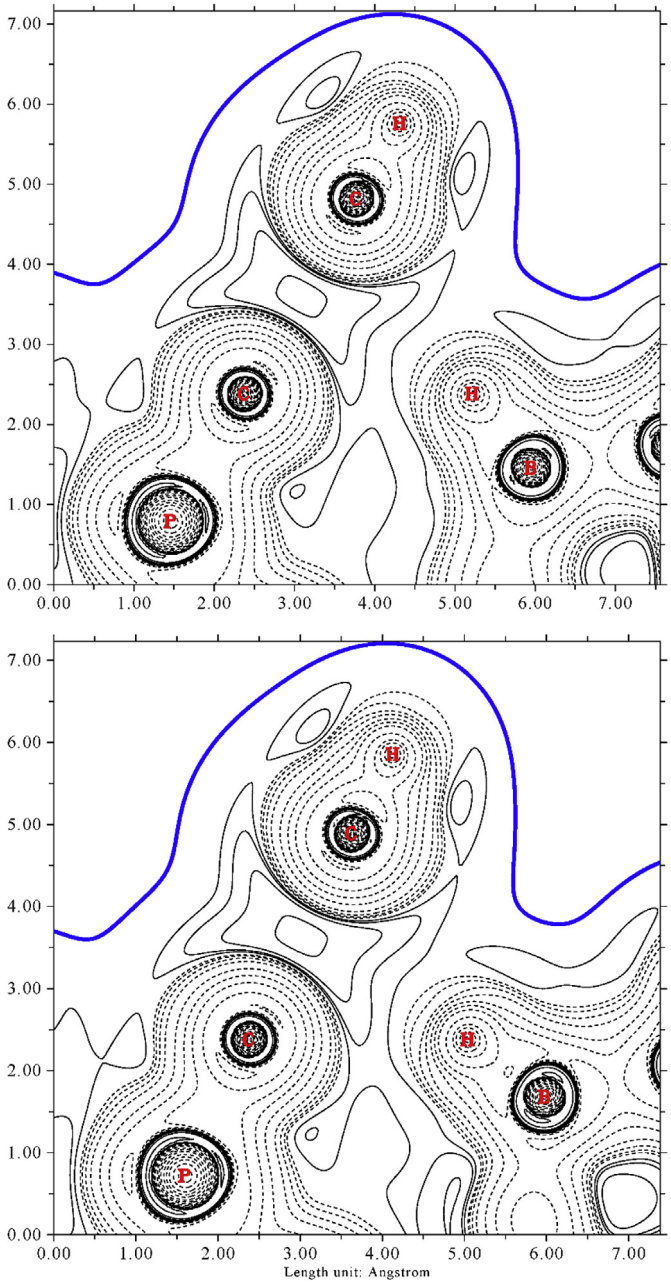

Fig. 7. Contour line diagram of the energy density H(r) calculated for **B1** (top) and **C1** (bottom) in the plane defined by the BH bond and the projection point of H in the plane of the neighboring phenyl ring that is shown in a sideward view so that only the P-C bond and the p-positioned C-H bond can be seen. Solid (dashed) contour lines indicate a positive (negative) energy density, whereas the blue line is the van der Waals isosurface with $\rho(r) = 0.001$ a.u. (For interpretation of the references to color in this figure legend, the reader is referred to the Web version of this article.)

matter whether the shortest distance to the ring plane or the distance to its center is taken (Table 1 in Reference [56]). As indicated by the θ angle defined in Fig. 9, the B-H bond in **Cn** points more to the C_6-ring than the analogue in **Bn** (see θ values in Table 1 of Reference [56]). This is a result of electron-withdrawing effects being present in the C-type carboranes opposed to electron-donating effects in the B-type analogues [103–106]. In this way B-H…π hydrogen bonds can be formed. H(B) is in all cases positively charged (0.06–0.09 e). Electron density and energy density have in all six complexes comparable values already discussed in connection with **B1** and **C1**.

The calculated local stretching force constants and the corresponding BSO values reflect the influence of the p-oriented substituent, which in the case of a methoxy group (**B3** and **C3**) is oriented in such a way that it can donate π density to the ring. This leads to a somewhat stronger B-H…π interaction and explains the increase in the BSO values from 0.348 to 0.359 and from 0.358 to 0.364, respectively (Table 1). The F atom is a much weaker π-donor and therefore a slight increase in the B-H…π interaction is only observed in the case of **C2** (Table 1 in Reference [56]).

The strength of the B-H…π H-bond is larger than that in **R12** (BSO: 0.247), which is the result of a close to optimal orientation of the B-H bond almost perpendicular to the plane of the neighboring phenyl ring as measured by the tilting angle θ in Fig. 9. Calculated θ values are between 9 and 22° and thereby not much different from the optimal value zero. We conclude that for the gas phase B-H…π H-bonds can be expected for the iridium complexes **B1**-**B3** and **C1**-**C3** investigated in this work.

4.3. Comparison with other recent investigations

Our findings about non-classical electrostatic B-H…π interactions [56] were recently challenged by some colleagues [107,108].

Grunenberg claims that his generalized compliance constants (which he calls relaxed force constants) may serve as unique bond-strength descriptors for classical and non-classical hydrogen bonds [107]. It has to be noted that at the energy minimum Grunenberg's relaxed force constants are equivalent to our local mode force constants [58]. Provided that the geometry optimization and the calculation of the Hessian have been made with the same methodology and high accuracy, the same stretching force constants will be obtained with both approaches. For example, our local B-H…π force constant of the **A4** system of 0.059 (Table 2 in Ref. [56]) compares well with Grunenberg's relaxed force constant value of 0.061 mDyn/Å (Table 1 in Ref. [107]). It is noteworthy that Grunenberg cites in his paper a value of 0.189 mDyn/Å for our B-H…π local force constant in **A4** (Table 1 in Ref. [107]), which is wrong and has never been reported by us. Therefore, there is no justification for his criticism of our work on the B-H…π interaction, which is based on an obviously erroneous citation. He is right in so far, that from an analysis of his coupling compliance constants, the description of B-H…π interactions as (classical or non-classical) hydrogen bonds is questionable. Coupling compliance constants are not physically based and depend on the coordinates being used for the description of the molecule [81]. In contrast, the sum of a local mode and its coupling frequency is always identical to the corresponding normal mode frequency, (established via an adiabatic coupling scheme), and therefore, is physically relevant [81].

Hobza, Lepsik et al. [108]. questioned our proof of concept of a new type of electrostatically driven nonclassical hydrogen bonding [56] arguing that such an explanation would contradict the wealth of evidence for unique noncovalent interactions of boron hydrides. They investigated the B-H…π interactions in closo-1,2-$C_2B_{10}H_{12}$ and closo-1,7-dehydro-$B_{12}H_{10}$ with benzene and hexafluorobenzene applying three methods including the ESP analysis, the restrained fit to the electrostatic potential (RESP) method, and DFT based symmetry-adapted perturbation theory (SAPT). These methods support the description of the B-H…π interaction as a nonspecific weak dispersion-driven B-H…π contact rather than as an electrostatically attractive nonclassical hydrogen bond.

However, some care has to be taken. These methods are no

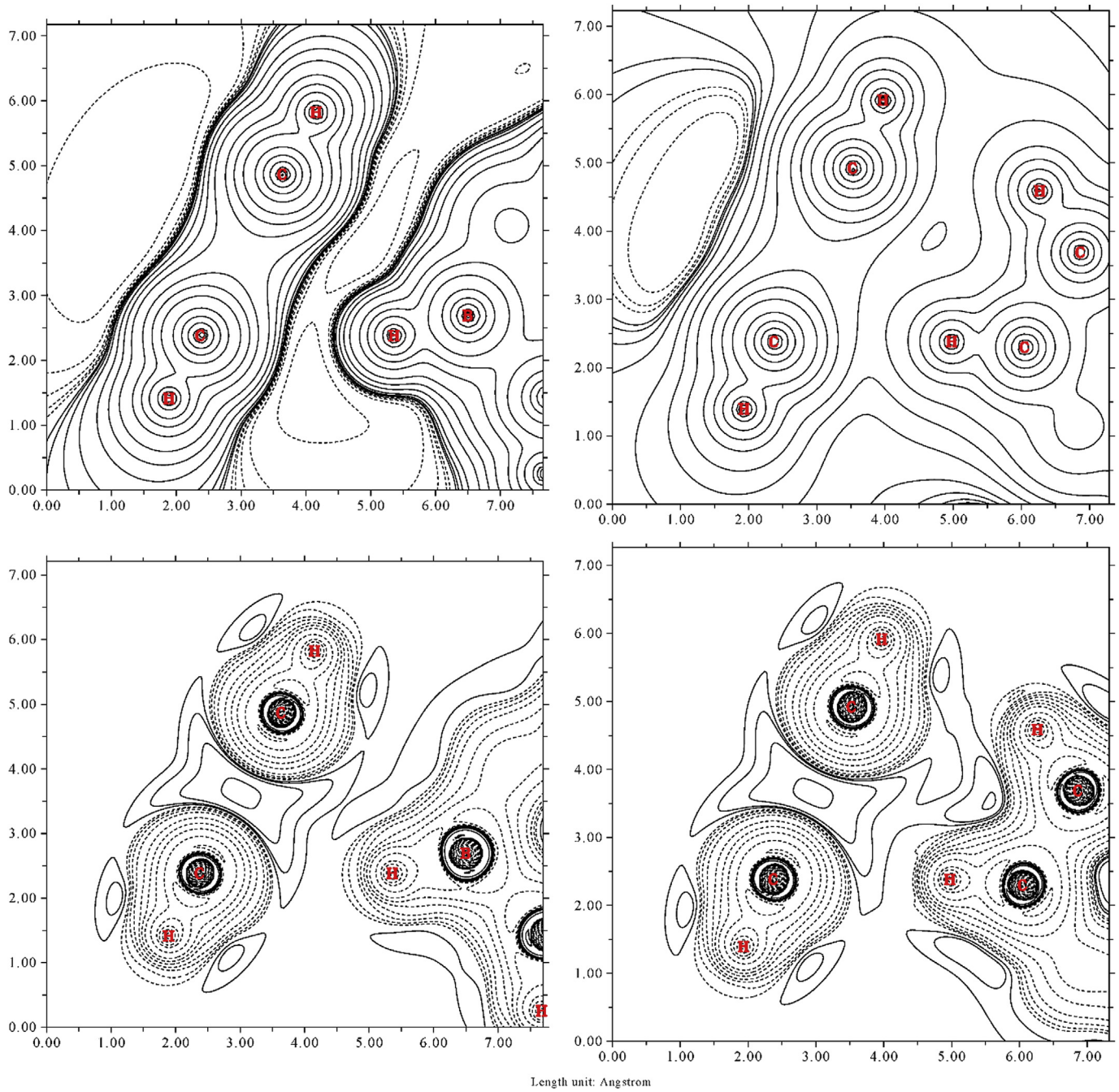

Fig. 8. Contour line diagrams of ESP calculated for the carborane-benzene complexes **R12** and **R13** (top left and right) in the plane of the BH (or CH) bond and the projection of the H atom in the benzene plane of which, in the sideward view, only two CH bonds can be seen. Solid (dashed) contour lines indicate a positive (negative) ESP value. In the lower half of the figure, contour line diagrams of the energy density.

universal approaches, and therefore they are not suited for deriving definite conclusions on a particular bonding situation.

1) The ESP is not a suitable tool for the quantitative analysis of B-H…π interactions, as shown in the previous section.
2) It is well known that all ESP-fitting charges (including the RESP charge used in Ref. [108]) suffer from the stability problem in the case of atoms being buried inside a molecule, which may lead to questionable atomic charges [109,110]. In addition to the NPA charges (see SI in Ref. [56]), we also calculated the Mulliken charges and the atomic dipole corrected Hirshfeld population (ADCH) [111] charges for the molecules listed in Table 1. Contrary to the ESP-fitting charges, all wave function-based charges qualitatively show that B (H) atoms facing the six-membered carbon ring are negatively (positively) charged, indicating the existence of electrostatic attractions between positively charged hydrogen atoms and negatively charged carbon atoms.
3) Both SAPT and the Energy Decomposition Analysis (EDA) can be applied to calculate dispersion ($E_{disp.}$) and electrostatic ($E_{e.s.}$) energies. DFT-SAPT [108] and our MP2-SAPT and MP2-LMOEDA results (not shown here) suggest that the dispersion energies are much stronger than their electrostatic counterparts in B-H…

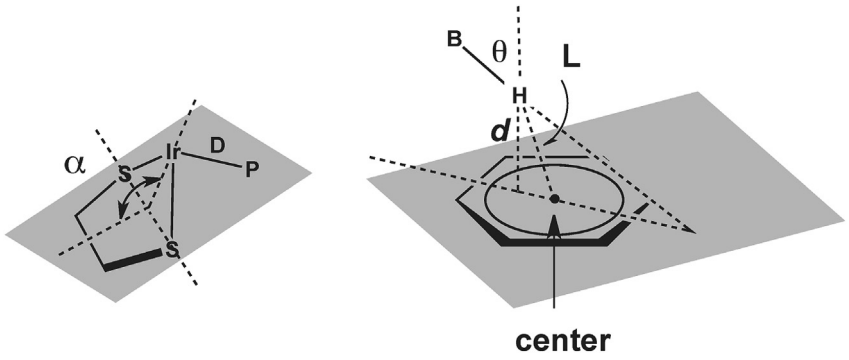

Fig. 9. Definition of distances d, D, L and angles α, θ used to characterize geometrical and conformational features of **B1**-**B3** and **C1**-**C3**.

π interactions. However, there are a number of non-classical bonds for which neither SAPT nor EDA provide conclusive results, as for example, the rare gas (Rg) bonds Rg-M in RgMX [112]. Our MP2-SAPT and MP2-LMOEDA test calculations led to $E_{e.s.} > 0$ and $E_{disp.} < 0$, pretending that the Rg-M bond may be a result of strong dispersions. However, both the topological electron density analysis [112] and the orbital analysis [113] revealed that the interactions are electrostatic (e.g. He-Be in HeBeO [112]) or may even be of covalent character (Xe-Au in XeAuF [112,113]). These counter examples clearly show a fatal defect, as reported by Frenking et al. [114]; *i.e.* the fragment charge dependence, which may lead to contrary conclusions, however has mostly been ignored so far. Usually neutral fragments are chosen as reference systems in the analyses, being different from the (more or less) charged fragments in actual molecular environment, therefore, may lead to unrealistic results. In addition, it has been frequently demonstrated in the literature that the division of electrostatic and dispersion interactions in EDA schemes is arbitrary to a certain extent and may lead to contradictory results [115–117]. Therefore, EDA/SAPT approaches may be questionable in particular in the case of weak polar bonding and C-H…π interactions, which are of hydrogen bond nature [117] and closely related to the B-H…π interactions investigated in this work. A large number of EDA and SAPT investigations insist that C-H…π interactions are dispersion dominated (e.g. see Ref. [118]) contradicting other work [117,119]. In conclusion, the usefulness of the SAPT or EDA analysis for the description of the delicate B-H…π interactions is also questionable.

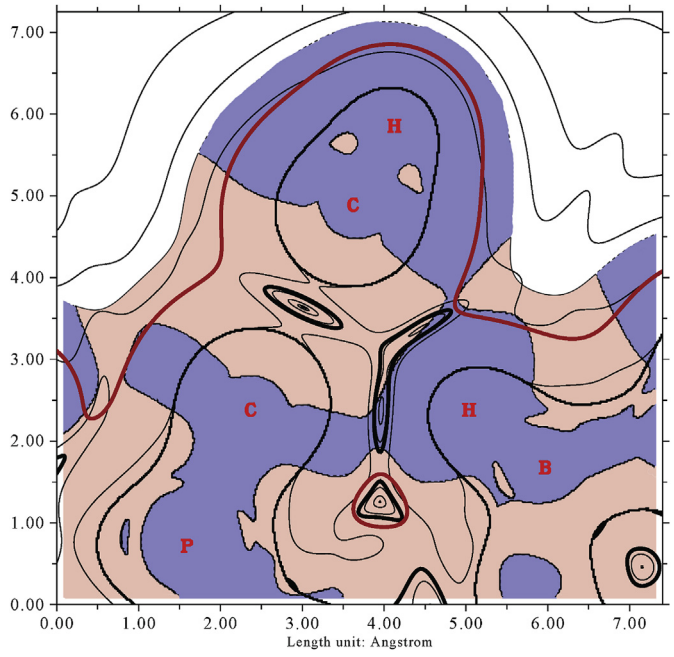

Fig. 10. Contour line diagram of RDG calculated for **C1** with the background of *t* values (light red for positive *t* and light blue for negative *t*). The bold black circle represents the RDG isosurface with $s = 0.5$ whereas the bold red circle for the density isosurface with $\rho = 0.005$ a.u. (For interpretation of the references to color in this figure legend, the reader is referred to the Web version of this article.)

4.4. The reduced density gradient (RDG) s

Yang et al. suggested the RDG *s* which is proportional to $|\nabla\rho|/\rho^{4/3}$ as a new tool for the characterization of noncovalent interactions [120]. Usually the isosurface with $s = 0.5$ and the values of $t = \text{sign}(\lambda_2)\rho$ on the surface (λ_2 is the second largest eigenvalue of the Hessian electronic density) is examined: a surface with $\rho < 0.005$ a.u. usually corresponds to dispersion interactions, whereas the one with $0.005 < \rho < 0.05$ a.u. and a negative (positive) λ_2 states stronger electrostatic interactions (steric clashes) [120]. In Fig. 10, the contour line diagram of RDG of **C1** with the *t* values in the background are plotted. It can be seen that there is an RDG isosurface with $s = 0.5$ between (B)H and the phenyl ring (R_{iso1}), which confirms the existence of a noncovalent interaction. Since the RDG isosurface fully lies within the region of $\rho > 0.005$ au, dispersion interactions can be excluded. It is interesting to see that the RDG isosurface passes through the boundary between electrostatic region (light blue) and steric clash region (light red). Due to a strong steric clash at the center of the phenyl ring (*i.e.* the RDG isosurface between two carbons; R_{iso2}), R_{iso1} is also affected, so there are some repulsive interactions in its center. However, at the edge of R_{iso1} electrostatic attraction becomes dominant, which agrees with our density topological analysis, since the (3,-1) critical point $\mathbf{r}_b$ is located near the center of R_{iso1}. The RDG analysis provides generally more insight into noncovalent interactions than the topological analysis, which is restricted to just a few critical points. SAPT and EDA approaches cannot distinguish between steric clashes and electrostatic attractions which coexist in a narrow area in B-H…π, so their results are not conclusive.

5. Experimental verification of a non-classical H-bond of the B-H…π type

We have synthesized the iridium complexes **B1**-**B3** and **C1**-**C3** according to procedures described in the following. In addition, we

synthesized the trimethylphosphine complexes **B4** and **C4** as suitable reference compounds that do not possess a BH…π H-bond.

5.1. Synthesis of complexes *B1-B4* and *C1-C4*

To a CH_2Cl_2 solution of [Cp*Ir($S_2C_2B_{10}H_{10}$)] (**B** or **C**) (107 mg, 0.2 mmol) PR_3 (0.2 mmol) was added and the mixture was stirred for 10 min at ambient temperature. The resulting yellow solution was evaporated *in vacuo* and the residue was washed with hexanes to give **B1-B4**, **C1-C4**, respectively. Single crystals suitable for X-ray analysis were obtained by slow evaporation of a CH_2Cl_2/hexane solution. (Note: for the preparation of **B4** and **C4**, slight excess of PMe_3 was added.)

5.1.1. [Cp*Ir(PPh$_3$)(9,12-$S_2C_2B_{10}H_{10}$)] (*B1*)

Yield: 94%. Color: yellow. m.p. 306–307 °C. ^{1}H {^{11}B} NMR ($CDCl_3$): δ 0.30 (s, 1H, cage-BH), 1.38 (d, 15H, J_{H-P} = 2 Hz, Cp*-CH_3), 1.70 (s, 2H, cage-BH), 2.04 (s, 4H, cage-BH), 2.11 (s, 1H, cage-BH), 2.54 (s, 2H, cage-CH), 7.33 (m, 9H, Ph), 7.72 (m, 6H, Ph); ^{11}B {^{1}H} NMR ($CDCl_3$): δ 18.7 (2B, B-S), −4.5 (2B), −11.4 (3B), −14.3 (3B); ^{31}P {^{1}H} NMR ($CDCl_3$): δ −2.23 (PPh_3); ^{13}C NMR ($CDCl_3$): δ 8.6 (Cp*-CH_3), 38.2 (cage-CH), 96.8 (Cp*-C), 127.1 (Ph), 128.6 (Ph), 133.4 (Ph), 135.4 (Ph). ESI-MS (positive ion mode) *m/z*: 819.11 (M+Na^+, 100%). IR (KBr): ω (cm^{-1}) 2558 (B-H), 2566 (B-H). Anal. Calcd. for $C_{30}H_{40}B_{10}PS_2Ir$: C, 45.26; H, 5.06. Found: C, 45.07; H, 5.23.

5.1.2. [Cp*Ir(PPh$_3$)(1,2-$S_2C_2B_{10}H_{10}$)] (*C1*)

Yield: 94%. Color: yellow solid. m.p. 317–318 °C. ^{1}H {^{11}B} NMR (CD_2Cl_2): δ 0.10 (s, 1H, cage-BH), 1.32 (s, 2H, cage-BH), 1.41 (d, J_{H-P} = 2 Hz, 15H, Cp*-CH_3), 1.96 (s, 1H, cage-BH), 2.02 (s, 3H, cage-BH), 2.08 (s, 1H, cage-BH), 2.50 (s, 2H, cage-BH), 7.42 (m, 9H, Ph), 7.50 (m, 6H, Ph); ^{11}B {^{1}H} NMR (CD_2Cl_2): δ −2.0 (1B), −5.8 (1B), −7.0 (2B), −9.7 (1B), −10.7 (2B), −11.8 (3B); ^{31}P {^{1}H} NMR ($CDCl_3$): δ 4.02 (PPh_3); ^{13}C NMR ($CDCl_3$): 8.9 (Cp*-CH_3), 90.3 (cage-C), 98.8 (Cp*-C), 127.7 (Ph), 129.6 (Ph), 134.4 (Ph), 134.4 (Ph). ESI-MS (positive ion mode) *m/z*: 819.06 (M+Na^+, 100%). IR (KBr): ω (cm^{-1}) 2578 (B-H). Anal. Calcd. for $C_{30}H_{40}B_{10}PS_2Ir$: C, 45.26; H, 5.06. Found: C, 45.02; H, 5.22.

5.1.3. [Cp*Ir(P(4-F-Ph)$_3$)(9,12-$S_2C_2B_{10}H_{10}$)] (*B2*)

Yield: 92%. Color: yellow solid. m.p. 280–281 °C. ^{1}H NMR ($CDCl_3$): δ ≈ 0.3 (1H, cage-BH), 1.40 (d, J_{H-P} = 2 Hz, 15H, Cp*-CH_3), 1.4–2.8 (7H, cage-BH), 2.60 (s, 2H, cage-CH), 7.03 (m, 6H, Ph), 7.67 (m, 6H, Ph); ^{11}B {^{1}H} NMR ($CDCl_3$): δ 18.5 (2B, B-S), −2.1 (2B), −11.8 (3B), −14.6 (3B); ^{31}P {^{1}H} NMR ($CDCl_3$): δ −2.47 [P(4-F-Ph)$_3$]; ^{13}C NMR ($CDCl_3$): δ 8.5 (Cp*-CH_3), 37.2 (cage-CH), 98.5 (Cp*-C), 114.4 (Ph), 134.5 (Ph), 138.0 (Ph), 163.0 (J_{C-F} = 250 Hz, Ph, C-F). ESI-MS (positive ion mode) *m/z*: 872.92 (M+Na^+, 100%). IR (KBr): ω (cm^{-1}) 2569 (B-H). Anal. Calcd. for $C_{30}H_{37}B_{10}F_3PS_2Ir$: C, 42.39; H, 4.39. Found: C, 42.10; H, 4.55.

5.1.4. [Cp*Ir(P(4-F-Ph)$_3$)(1,2-$S_2C_2B_{10}H_{10}$)] (*C2*)

Yield: 93%. Color: yellow solid. m.p. 288–289 °C. ^{1}H NMR ($CDCl_3$): δ ≈ 0.0 (1H, cage-BH), 1.45 (d, J_{H-P} = 2 Hz, 15H, Cp*-CH_3), 1.3–3.0 (9H, cage-BH), 7.12 (m, 6H, Ph), 7.46 (m, 6H, Ph); ^{11}B {^{1}H} NMR ($CDCl_3$): δ −1.7 (1B), −5.2 (1B), −6.6 (2B), −10.1 (3B), −11.8 (3B); ^{31}P {^{1}H} NMR ($CDCl_3$): δ −2.56 [P(4-F-Ph)$_3$]; ^{13}C NMR ($CDCl_3$): δ 8.8 (Cp*-CH_3), 89.3 (cage-C), 98.5 (Cp*-C), 115.3 (Ph), 134.6 (Ph), 137.4 (Ph), 163.4 (J_{C-F} = 250 Hz, Ph, C-F). ESI-MS (positive ion mode) *m/z*: 873.00 (M+Na^+, 100%). IR (KBr): ω (cm^{-1}) 2578 (B-H). Anal. Calcd. for $C_{30}H_{37}B_{10}F_3PS_2Ir$: C, 42.39; H, 4.39. Found: C, 42.12; H, 4.63.

5.1.5. [Cp*Ir(P(4-OMe-Ph)$_3$)(9,12-$S_2C_2B_{10}H_{10}$)] (*B3*)

Yield: 91%. Color: yellow solid. m.p. 277–278 °C. ^{1}H NMR ($CDCl_3$): δ ≈ 0.3 (1H, cage-BH), 1.37 (d, J_{H-P} = 2 Hz, 15H, Cp*-CH_3), 1.4–2.8 (7H, cage-BH), 2.36 (s, 2H, cage-CH), 3.85 (s, 9H, OMe), 7.03 (m, 6H, Ph), 7.67 (m, 6H, Ph); ^{11}B {^{1}H} NMR ($CDCl_3$): δ 16.3 (2B, B-S), −4.5 (2B), −11.8 (3B), −14.7 (3B); ^{31}P {^{1}H} NMR ($CDCl_3$): δ −2.12 [P(4-OMe-Ph)$_3$]; ^{13}C NMR ($CDCl_3$): δ 8.4 (Cp*-CH_3), 39.4 (cage-CH), 55.2 (OCH_3), 98.7 (Cp*-C), 113.2 (Ph), 113.9 (Ph), 133.9 (Ph), 136.1(Ph); ESI-MS (positive ion mode) *m/z*: 909.10 (M+Na^+, 100%). IR (KBr): ω (cm^{-1}) 2555 (B-H). Anal. Calcd. for $C_{33}H_{46}B_{10}PS_2IrO_3$: C, 44.73; H, 5.23. Found: C, 44.61; H, 5.40.

5.1.6. [Cp*Ir(P(4-OMe-Ph)$_3$)(1,2-$S_2C_2B_{10}H_{10}$)] (*C3*)

Yield: 91%. Color: yellow solid. m.p. 285–286 °C. ^{1}H NMR ($CDCl_3$): δ ≈ 0.0 (1H, cage-BH), 1.44 (d, J_{H-P} = 2 Hz, 15H, Cp*-CH_3), 1.3–3.0 (9H, cage-BH), 3.85 (s, 9H, OMe), 6.89 (m, 6H, Ph), 7.40 (m, 6H, Ph); ^{11}B {^{1}H} NMR ($CDCl_3$): δ −1.6 (1B), −5.6 (1B), −7.0 (2B), −10.6 (3B), −12.0 (3B); ^{31}P {^{1}H} NMR ($CDCl_3$): δ −0.34 [P(4-OMe-Ph)$_3$]; ^{13}C NMR ($CDCl_3$): δ 8.8 (Cp*-CH_3), 55.4 (OCH_3), 85.8 (cage-C), 98.3 (Cp*-C), 113.3 (Ph), 114.5 (Ph), 134.6 (Ph), 136.8 (Ph); ESI-MS (positive ion mode) *m/z*: 909.10 (M+Na^+, 100%). IR (KBr): ω (cm^{-1}) 2569 (B-H). Anal. Calcd. for $C_{33}H_{46}B_{10}PS_2IrO_3$: C, 44.73; H, 5.23. Found: C, 44.59; H, 5.37.

5.1.7. [Cp*Ir(PMe$_3$)(9,12-$S_2C_2B_{10}H_{10}$)] (*B4*)

Yield: 98%. Color: yellow solid. m.p. 278–279 °C. ^{1}H {^{11}B} NMR ($CDCl_3$): δ 1.68 (d, J_{H-P} = 11 Hz, 9H, P-CH_3), 1.72 (d, J_{H-P} = 2 Hz, 15H, Cp*-CH_3), 2.03 (s, 2H, cage-BH), 2.13 (s, 2H, cage-BH), 2.18 (s, 2H, cage-BH), 2.34 (s, 1H, cage-BH), 2.71 (s, 2H, cage-CH), 2.81 (s, 1H, cage-BH); ^{11}B {^{1}H} NMR ($CDCl_3$): δ 16.0 (2B, B-S), −5.1 (2B), −14.3 (3B), −17.3 (3B); ^{31}P {^{1}H} NMR ($CDCl_3$): δ −29.5 (PMe_3); ^{13}C NMR ($CDCl_3$): δ 9.1 (Cp*-CH_3), 16.3 (PMe_3), 90.5 (cage-C), 97.4 (Cp*-C). ESI-MS (positive ion mode) *m/z*: 634.08 (M+Na^+, 100%). IR (KBr): ω (cm^{-1}) 2559, (B-H), 2568 (B-H). Anal. Calcd. for $C_{15}H_{34}B_{10}PS_2Ir$: C, 29.52; H, 5.57. Found: C, 29.23; H, 5.72.

5.1.8. [Cp*Ir(PMe$_3$)(1,2-$S_2C_2B_{10}H_{10}$)] (*C4*)

Yield: 97%. Color: yellow solid. m.p. 286–287 °C. ^{1}H {^{11}B} NMR ($CDCl_3$): 1.59 (s, 2H, cage-BH), δ 1.66 (d, J_{H-P} = 11 Hz, 9H, P-CH_3), 1.77 (d, J_{H-P} = 2 Hz, 15H, Cp*-CH_3), 2.06 (s, 1H, cage-BH), 2.14 (s, 1H, cage-BH), 2.43 (s, 3H, cage-BH), 2.66 (s, 2H, cage-BH); 2.98 (s, 1H, cage-BH); ^{11}B {^{1}H} NMR ($CDCl_3$): δ −1.5 (1B), −5.3 (2B), −6.1 (2B), −9.7 (3B), −11.5 (2B); ^{31}P {^{1}H} NMR ($CDCl_3$): δ −26.0 (PMe_3); ^{13}C NMR ($CDCl_3$): δ 8.9 (Cp*-CH_3), 16.1 (P-CH_3), 37.14 (cage-C), 94.0 (Cp*-C). ESI-MS (positive ion mode) *m/z*: 634.18 (M+Na^+, 100%). IR (KBr): ω (cm^{-1}) 2592 (B-H).

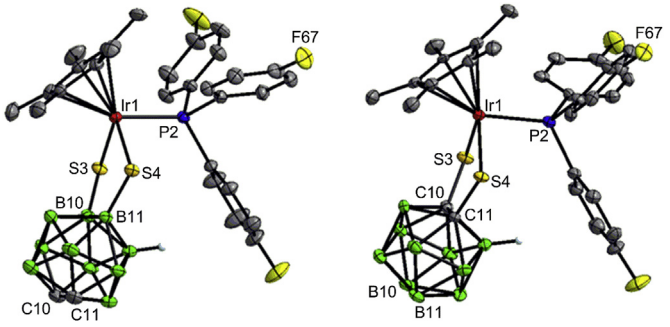

Fig. 11. X-ray structures of the folded conformers of **B2** and **C2**. The assumed position of the interacting H(B) atom is shown. (Color code: C: grey; B: green; F: yellow; P: blue; S: orange; Ir: red.). (For interpretation of the references to color in this figure legend, the reader is referred to the Web version of this article.)

5.2. Structure of complexes *B1-B4* and *C1-C3*

The structures of the Ir-complexes synthesized were verified and characterized with the help of the X-ray diffraction analyses (CCDC number: 1014546, 1014547, 1014549, 1014550, 1014551, 1014553, 1059257). As an example, the ball & stick representations of complexes **B2** and **C2** are shown in Fig. 11 where the assumed position of the (B)-H interacting with a phenyl ring is indicated (see SI for coordinates). The X-ray structures confirm the tilting of the Cp^* ligand, the propeller-like arrangement of the phenyl groups and features of the five-membered ring, which adopts an envelope form with a folding angle α of 157 ± 1° (calculated) or 157.5 ± 1.5° (X-ray diffraction measurements).

A comparison of calculated gas-phase and X-ray diffraction (solid state) structures leads to a close agreement as is reflected by the bond lengths listed in Table S2 of SI in Ref. [56]. Also, the structural parameters α, θ, D, d, and L defined in Fig. 9 and used to analyze the steric interactions between phenyl groups and the closest B-H bond of the $S_2C_2B_{10}H_{10}$ ligand are all in reasonable agreement (Table 1 in Ref. [56]).

In addition, we verified the existence of the intramolecular B-H…π interactions in solution using NMR spectroscopy. The titration of a solution of host **B** in $CDCl_3$ with PPh_3 (**1**) led to a new Cp^* proton signal in the ^1H NMR spectrum, which could be assigned to the conformer **B1**. For all cases, the methyl singlets of **B1-B3** and **C1-C3** were shifted up-field by ca. 0.50 ppm compared to the corresponding signals measured for the hosts **B** or **C** thus indicating the formation of $[Cp^*Ir(PR_3)S_2C_2B_{10}H_{10}]$ complexes in solution. Furthermore, a low-frequency shifting of the B-H resonance signals was observed upon addition of PPh_3 to solutions of **B** or **C** (see, e.g., Fig. S11(a) of SI in Ref. [56]). Similar NMR results have also been observed in the case of B-H-metal interactions [121–123]. By comparison, reference complexes **B4** and **C4** in which a B-H…π interaction cannot form, had normal B-H resonance signals (1.8–3.2 ppm). These results suggest the formation of B-H…π H-bonds in $[Cp^*Ir(PR_3)S_2C_2B_{10}H_{10}]$ complexes in solution.

Although the experimental evidence is in line with the existence of the B-H…π H-bond, they cannot provide indisputable results because the positions of the H atoms are estimated and packing effects in the solid state hinder to extract electronic trends caused by the p-phenyl substituents of the phosphine ligand, which would provide more direct evidence for H-bonding. The situation becomes more complicated by the fact that **B3** and **C2** exist in the unit cell in form of dimers.

5.3. Investigation of the dimers of *B3* and *C2*

The dimers of **B3** and **C2** are stabilized by non-covalent interactions leading to complex binding energies of −23.4 and −12.2 kcal/mol, respectively. The significantly higher binding energy for the dimer of **B3** is a result of the propeller-to-propeller interaction of the monomers where CH bonds of the phenyl rings and the methoxy groups interact with the π-system of the other monomer as indicated in SI, pp. S50. In the case of the dimer of **C2** (see SI in Ref. [56], pp. S55). the binding energy is a result of the non-covalent interactions between the methyl groups of the Cp^* ligand of the right monomer and the phenyl rings of the left monomer (distance between the H atoms and ring: ca. 2.5 Å). A direct propeller-propeller interaction as in the case of the **B3**-dimer seems to be hindered because of the F-substituents in the p-positions of **C2**, which lead to exchange repulsion in this configuration, but are in positions without negatively charged counterparts in close proximity when the Cp^*-propeller configuration (see SI in Ref. [56], pp. S55) is chosen. In principle, the arrangement in the **C2**-dimer can be extended to long strings of molecules with a zig-zagging structure, which is not possible in the propeller-to-propeller arrangement of dimer **B3**. In so far, the latter dimer can be used as a terminating group for any molecular string made up by dimers of **C2**. We note that the non-classical BH H-bond stabilizes the propeller-like arrangement of the phosphine substituents, which in turn can be used for the generation of (a)cyclic oligomers interesting in connection with materials science.

Irrespective of the dimer configuration, the B-H…π H-bond is retained (H46 at right side and atom H42 on the left side of the dimer **B3** in SI in Ref. [56], pp. S50; H46 at the right side and atom H30 on the left side of the dimer of **C2**, pp. S55 of SI in Ref. [56]). Measured and calculated geometries of the dimers as well as the NPA charges of the two dimers are given in SI in Ref. [56].

6. Conclusions

In this work, the existence of a B-H…π H-bond has been proved for the first time for Ir complexes **B1**-**B3** and **C1**-**C3** by a multi-pronged approach:

i) The existence of this kind of non-classical H-bond has been verified by reliable quantum chemical calculations. A molecular template in form of an iridium complex has been developed that provides a basis of observing B-H…π H-bonding. Suitable quantum chemical tools in form of the energy density distribution and the local stretching force constant k_a(H … π) confirm the existence of this type of H-bonding for the iridium complexes in question. Predictions are valid for the gas phase.

ii) To verify the existence of B-H…π H-bonding for the solid state, the six iridium complexes **B1**-**B3** and **C1**-**C3** were synthesized and their structure was obtained with the help of X-ray diffraction analyses. The propeller-type arrangement of the phosphinephenyl substituents predicted by the calculations was confirmed. The proximity of the carborane group and one phenyl substituent makes B-H…π H-bonding likely. A general agreement was obtained between measured and calculated structural parameters, both for type **B** and type **C**-iridium complexes.

iii) NMR chemical shift measurements for complexes **B1**-**B3** and **C1**-**C3** in solution revealed that one BH signal is high field shifted thus indicating that the corresponding proton is shielded by the ring current of a near-by phenyl ring. The signal could no longer be observed if the formation of a B-H…π H-bond is prevented by using a trialkyl phosphine as bonding partner for the 16e complexes **B** or **C.**

Hence, the B-H…π H-bond for gas, solution, and solid phase of the iridium complexes **B1**-**B3** and **C1**-**C3** was indisputably verified. We note that such interactions do not exist in the case of a BH_3-benzene complex, as was first suggested by Tarakeshwar and co-workers [10]. The detection of a B-H…π H-bond in **R9** or between carborane and benzene is only possible at low temperatures as was shown in this work by the calculation of the corresponding free energy differences (Fig. 1). It was also shown that the B-H…π H-bond has a stability comparable to that of the H-bond in the water dimer [59] according to the calculated binding energies, local stretching force constants, and BSO values.

In the case of the dimers of **B3** and **C2**, binding energies of −23.4 and −12.2 kcal/mol were predicted. A propeller-to-propeller interaction between the phenyl groups of the **B3**-dimer causes increased stability. For **C2**, there are only the non-covalent interactions between the methyl groups of the Cp^* ligand of one monomer and the phenyl rings of the other monomer possible

because the propeller-to-propeller interactions lead to destabilizing interactions involving the F substituents.

iv) The B-H…π H-bond can be found in the B_2H_6…benzene complex **R9.** Its stability is similar to that of the water dimer (−5.1 compared to −5.0 kcal/mol [59]), i.e. this complex can only be observed at low temperatures. The stability of $C_2B_{10}H_{12}$-benzene is even smaller (−3.9 kcal/mol) because the angle θ between the BH bond and the normal of the benzene plane is 42°.

The experimental realization of a B-H…π H-bond was successful due to the enhancement of steric crowding involving a phenyl-substituted phosphine and a bidentated $S_2C_2B_{10}H_{10}$ ligand. Both X-ray and quantum chemical calculations revealed that the typical (B)H-benzene distance d is 2.4–2.5 Å. B-H…π H-bonds are electrostatic in nature and, similar to C-H…π H-bonds. They can stabilize a preferred conformation of a transition metal complex or dimer.

v) The EPS is not a suitable tool for the verification of the B-H…π H-bond, because the density in this region is considerable larger than 0.001 a.u., and therefore strongly influenced by the positive nuclear charge overpowering the contribution of the negative electronic charge. The existence of the B-H…π H-bond can be confirmed by the topological analysis of the electron density distribution with the energy density H(**r**) as an indicator: The B-H…π H-bond is a result of an electrostatic attraction between an electrophilic region with negative H(**r**) and a nucleophilic region with positive H(**r**).

vi) A more detailed inspection by the RDG analysis confirmed that B-H…π H-bonds are electrostatic in nature, although there are also some steric clashes. The coexistence of steric clashes and electrostatic attractions in B-H…π makes the SAPT and EDA results questionable.

Acknowledgment

At SMU, the work was financially supported by the National Science Foundation, Grants CHE 1152357 and CHE 1464906. We thank SMU for providing computational resources. At Nanjing, this work was supported by the National Natural Science Foundation (21472086 and 21531004). We also thank the High Performance Computing Center of Nanjing University for providing computational resources. At last, we thank the unknown reviewers for valuable suggestions.

Appendix A. Supplementary data

Supplementary data related to this article can be found at https://doi.org/10.1016/j.jorganchem.2018.02.014.

References

[1] E.A. Meyer, R.K. Castellano, F. Diederich, Angew. Chem. Int. Ed. 42 (2003) 1210–1250.
[2] O. Takahashi, Y. Kohno, M. Nishio, Chem. Rev. 110 (2010) 6049–6076.
[3] L. Berg, B.K. Mishra, C.D. Andersson, F. Ekstrom, Anna Linusson, Chem. Eur J. 22 (2016) 2672–2681.
[4] J.C. Lopez, W. Caminati, J.L. Alonso, Angew. Chem. Int. Ed. 45 (2006) 290–293.
[5] S. Tsuzuki, K. Honda, T. Uchimaru, M. Mikami, K. Tanabe, J. Phys. Chem. A 106 (2002) 4423–4428.
[6] D.A. Rodham, S. Suzuki, R.D. Suenram, F.J. Lovas, S. Dasgupta, W.A. Goddard III, G.A. Blake, Nature 362 (1993) 735–737.
[7] S. Vaupel, B. Brutschy, P. Tarakeshwar, K.S. Kim, J. Am. Chem. Soc. 128 (2006) 5416–5426.
[8] S. Suzuki, P.G. Green, R.E. Bumgarner, S. Dasgupta, W.A. Goddard III, G.A. Blake, Science 257 (1992) 942–945.
[9] R.N. Pribble, T.S. Zwier, Science 265 (1994) 75–79.
[10] P. Trarakeshwar, H.S. Choi, K.S. Kim, J. Am. Chem. Soc. 123 (2001) 3323–3331.
[11] H. Li, D. Min, S.G. Shore, W.N. Lipscomb, W. Yang, Inorg. Chem. 46 (2007) 3956–3959.
[12] S.X. Tian, H.-B. Li, Y. Bai, J. Yang, J. Phys. Chem. A 112 (2008) 8121–8128.
[13] R. Sedlák, J. Fanfrlík, D. Hnyk, P. Hobza, M. Lepšík, J. Phys. Chem. A 114 (2010) 11304–11311.
[14] P. Ravinder, V. Subramanian, J. Phys. Chem. A 114 (2010) 5565–5572.
[15] J.W.G. Bloom, R.K. Raju, S.E. Wheeler, J. Chem. Theor. Comput. 8 (2012) 3167–3174.
[16] W.W. Porterfield, Inorganic Chemistry: a Unified Approach, Academic Press, San Diego, 1993.
[17] K. Wade, Electron Deficient Compounds, Meredith Corporation, New York, 1993.
[18] N.S. Hosmane, Boron Science: New Technologies and Applications, CRC Press, Boca Raton, 2011.
[19] R.N. Grimes, Carboranes, second ed., Elsevier, 2011.
[20] M.F. Hawthorne, Angew. Chem. Int. Ed. 32 (1993) 950–984.
[21] V.I. Bregadze, I.B. Sivaev, S.A. Glazun, Anti Canc. Agents Med. Chem. 6 (2006) 75–109.
[22] F. Issa, M. Kassiou, L.M. Rendina, Chem. Rev. 111 (2011) 5701–5722.
[23] M. Scholz, E. Hey-Hawkins, Chem. Rev. 111 (2011) 7035–7062.
[24] N.P.E. Barry, P.J. Sadler, Chem. Soc. Rev. 41 (2012) 3264–3279.
[25] J. Plesek, Chem. Rev. 92 (1992) 269–278.
[26] V.I. Bregadze, Chem. Rev. 92 (1992) 209–223.
[27] A.K. Saxena, J.A. Maguire, N.S. Hosmane, Chem. Rev. 97 (1997) 2421–2462.
[28] B.P. Dash, R. Satapathy, E.R. Gaillard, J.A. Maguire, N.S. Hosmane, J. Am. Chem. Soc. 132 (2010) 6578–6587.
[29] K.R. Wee, Y.J. Cho, J.K. Song, S.O. Kang, Angew. Chem. Int. Ed. 52 (2013) 9682–9685.
[30] C. Shi, H. Sun, X. Tang, H. Lv, H. Yan, Q. Zhao, J. Wang, W. Huang, Angew. Chem. Int. Ed. 52 (2013) 13434–13438.
[31] C. Shi, H. Sun, Q. Jiang, Q. Zhao, J. Wang, W. Huang, H. Yan, Chem. Commun. 49 (2013) 4746–4748.
[32] C. Masalles, J. Llop, F. Teixidor, Adv. Mater. 14 (2002) 826–829.
[33] J. Mola, E. Mas-Marza, X. Sala, I. Romero, M. Rodriguez, C. Vinas, T. Parella, A. Llobet, Angew. Chem. Int. Ed. 47 (2008) 5830–5832.
[34] P. Farras, F. Teixidor, I. Rojo, R. Kivekäs, R. Sillanpää, P. Gonzalez-Cardoso, C. Vinas, J. Am. Chem. Soc. 133 (2011) 16537–16552.
[35] A.M. Cioran, A.D. Musteti, F. Teixidor, Z. Krpetic, I.A. Prior, Q. He, C.J. Kiely, M. Brust, C. Viñas, J. Am. Chem. Soc. 134 (2012) 212–221.
[36] M. Tominaga, Y. Morisaki, Y. Chujo, Macromol. Rapid Commun. 34 (2013) 1357–1362.
[37] Y. Morisaki, M. Tomiaga, T. Ochiai, Y. Chujo, Chem. Asian J. 9 (2014) 1247–1251.
[38] N.S. Hosmane, J.A. Maguire, in: R.H. Crabtree, D.M.P. Mingos (Eds.), Comprehensive Organometallic Chemistry III, Elsevier, Oxford, 2007, pp. 175–264.
[39] Z. Xie, Acc. Chem. Res. 36 (2003) 1–9.
[40] L. Deng, Z. Xie, Coord. Chem. Rev. 251 (2007) 2452–2476.
[41] S. Liu, Y.F. Han, G.X. Jin, Chem. Soc. Rev. 36 (2007) 1543–1560.
[42] Z. Qiu, S. Ren, Z. Xie, Acc. Chem. Res. 44 (2011) 299–309.
[43] Z. Xie, G.X. Jin, Dalton Trans. 43 (2014) 4924.
[44] P. Cigler, M. Kozisek, P. Rezacova, J. Brynda, Z. Otwinowski, J. Pokorna, J. Plesek, B. Grlźner, L. Doleckova-Maresova, M. Masa, J. Sedlacek, J. Bodem, H. Krausslich, V. Kral, J. Konvalinka, PNAS 102 (2005) 15394–15399.
[45] P.D. Godfrey, W.J. Grigsby, P.J. Nichols, C.L. Raston, Chem. Eur J. 10 (2004) 279–282.
[46] M.J. Hardie, C.L. Raston, Chem. Commun. (1999) 1153–1163.
[47] C.A. Reed, Acc. Chem. Res. 31 (1998) 133–139.
[48] J.G. Planas, C. Vinas, F. Teixidor, A. Coms-Vives, G. Ujaque, A. Lledos, M.E. Light, M.B. Hursthouse, J. Am. Chem. Soc. 127 (2005) 15976–15982.
[49] Z.J. Yao, W.B. Yu, Y.J. Lin, S.L. Huang, Z.H. Li, G.X. Jin, J. Am. Chem. Soc. 136 (2014) 2825–2832.
[50] M.A. Fox, A.K. Hughes, Coord. Chem. Rev. 248 (2004) 457–476.
[51] H. Lee, C.B. Knobler, M.F. Hawthorne, Chem. Commun. (2000) 2485–2486.
[52] M.J. Bayer, A. Herzog, M. Diaz, G.A. Harakas, H. Lee, C.B. Knobler, M.F. Hawthorne, Chem. Eur. J. 9 (2003) 2732–2744.
[53] M.J. Hardie, P.D. Godfrey, C.L. Raston, Chem. Eur. J. 5 (1999) 1828–1833.
[54] M.J. Hardie, C.L. Raston, Eur. J. Inorg. Chem. (1999) 195–200.
[55] C.L. Raston, J. Cave, Chem. Eur. J. 10 (2004) 279–282.
[56] X. Zhang, H. Dai, H. Yan, W. Zou, D. Cremer, J. Am. Chem. Soc. 138 (2016) 4334–4337.
[57] Z. Konkoli, D. Cremer, Int. J. Quant. Chem. 67 (1998) 1–9.
[58] W. Zou, E. Kalescky, E. Kraka, D. Cremer, J. Chem. Phys. 137 (2012), 084114.
[59] R. Kalescky, W. Zou, E. Kraka, D. Cremer, Chem. Phys. Lett. 554 (2012) 243–247.
[60] M. Freindorf, E. Kraka, D. Cremer, Int. J. Quant. Chem. 112 (2012) 3174–3187.
[61] R. Kalescky, E. Kraka, D. Cremer, J. Phys. Chem. A 117 (2013) 8981–8995.
[62] D. Cremer, E. Kraka, Croat. Chem. 57 (1984) 1259–1281.
[63] D. Cremer, E. Kraka, Angew Chem. Int. Ed. Engl. 23 (1984) 627–628.
[64] E. Kraka, D. Cremer, Chemical Implications of Local Features of the Electron Density Distribution, vol. 2, Springer-Verlag, Heidelberg, 1990, pp. 457–542.
[65] J.-D. Chai, M. Head-Gordon, Phys. Chem. Chem. Phys. 10 (2008) 6615–6620.
[66] J.-D. Chai, M. Head-Gordon, J. Chem. Phys. 128 (2008), 084106.
[67] K. Raghavachari, G.W. Trucks, J.A. Pople, M. Head-Gordon, Chem. Phys. Lett. 157 (1989) 479–483.

[68] K. Thanthiriwatte, E. Hohenstein, L. Burns, C. Sherrill, J. Chem. Theor. Comput. 7 (2011) 88–96.
[69] F. Weigend, R. Ahlrichs, Phys. Chem. Chem. Phys. 7 (2005) 3297–3305.
[70] P. Hariharan, J. Pople, Theor. Chim. Acta 28 (1973) 213–222.
[71] T. Clark, J. Chandrasekhar, G.W. Spitznagel, P.V.R. Schleyer, J. Comput. Chem. 4 (1983) 294–301.
[72] J. Gräfenstein, D. Cremer, J. Chem. Phys. 127 (2007) 164113.
[73] S. Boys, F. Bernardi, Mol. Phys. 19 (1970) 553–566.
[74] A. Reed, L. Curtiss, F. Weinhold, Chem. Rev. 88 (1988) 899–926.
[75] F. Weinhold, C.R. Landis, Valency and Bonding: a Natural Bond Orbital Donor-acceptor Perspective, Cambridge University Press, Cambridge, UK, 2003.
[76] R.F.W. Bader, M.T. Carroll, J.R. Cheeseman, C. Chang, J. Am. Chem. Soc. 109 (1987) 7968–7979.
[77] R.F.W. Bader, Atoms in Molecules-a Quantum Theory, Oxford University Press, Oxford, UK, 1990.
[78] E.B. Wilson, J.C. Decius, P.C. Cross, Molecular Vibrations. The Theory of Infrared and Raman Vibrational Spectra, McGraw-Hill, New York, 1955.
[79] W. Zou, D. Cremer, Theor. Chem. Acc. 133 (2014) 1451.
[80] W. Zou, R. Kalescky, E. Kraka, D. Cremer, J. Mol. Model. 19 (2013) 2865–2877.
[81] R. Kalescky, W. Zou, E. Kraka, D. Cremer, J. Phys. Chem. A 118 (2014) 1948–1963.
[82] E. Kraka, J.A. Larsson, D. Cremer, in: J. Grunenberg (Ed.), Computational Spectroscopy: Methods, Experiments and Applications, Wiley, New York, 2010, pp. 105–149.
[83] R. Kalescky, E. Kraka, D. Cremer, J. Phys. Chem. A 118 (2014) 223–237.
[84] W. Zou, D. Cremer, Chem. Eur J. 22 (2016) 4087–4099.
[85] D. Setiawan, E. Kraka, D. Cremer, J. Comput. Chem. 37 (2016) 130–142.
[86] R. Kalescky, E. Kraka, D. Cremer, Mol. Phys. 111 (2013) 1497–1510.
[87] R.M. Badger, J. Chem. Phys. 2 (1934) 128–131.
[88] R.M. Badger, J. Chem. Phys. 3 (1935) 710–715.
[89] E. Kraka, W. Zou, M. Filatov, J. Grafenstein, D. Izotov, J. Gauss, Y. He, A. Wu, Z. Konkoli, V. Polo, L. Olsson, Z. He, D. Cremer, COLOGNE2016, 2014. http://www.smu.edu/catco. (Accessed 24 December 2017).
[90] M.J. Frisch, G.W. Trucks, H.B. Schlegel, G.E. Scuseria, M.A. Robb, J.R. Cheeseman, G. Scalmani, V. Barone, B. Mennucci, G.A. Petersson, H. Nakatsuji, M. Caricato, X. Li, H.P. Hratchian, A.F. Izmaylov, J. Bloino, G. Zheng, J.L. Sonnenberg, M. Hada, M. Ehara, K. Toyota, R. Fukuda, J. Hasegawa, M. Ishida, T. Nakajima, Y. Honda, O. Kitao, H. Nakai, T. Vreven, J.A. Montgomery Jr., J.E. Peralta, F. Ogliaro, M. Bearpark, J.J. Heyd, E. Brothers, K.N. Kudin, V.N. Staroverov, T. Keith, R. Kobayashi, J. Normand, K. Raghavachari, A. Rendell, J.C. Burant, S.S. Iyengar, J. Tomasi, M. Cossi, N. Rega, J.M. Millam, M. Klene, J.E. Knox, J.B. Cross, V. Bakken, C. Adamo, J. Jaramillo, R. Gomperts, R.E. Stratmann, O. Yazyev, A.J. Austin, R. Cammi, C. Pomelli, J.W. Ochterski, R.L. Martin, K. Morokuma, V.G. Zakrzewski, G.A. Voth, P. Salvador, J.J. Dannenberg, S. Dapprich, A.D. Daniels, O. Farkas, J.B. Foresman, J.V. Ortiz, J. Cioslowski, D.J. Fox, Gaussian 09, Revision D.01, Gaussian, Inc., Wallingford CT, 2013.
[91] T. Lu, F. Chen, J. Comput. Chem. 33 (2012) 580–592.
[92] B. Jeziorski, R. Moszynski, K. Szalewicz, Chem. Rev. 94 (1994) 1887–1930.
[93] E.G. Hohenstein, R.M. Parrish, C.D. Sherrill, J.M. Turney, H.F. Schaefer, J. Chem. Phys. 135 (2011) 174017.
[94] P. Su, H. Li, J. Chem. Phys. 131 (2009), 014102.
[95] J.M. Turney, A.C. Simmonett, R.M. Parrish, E.G. Hohenstein, F. Evangelista, J.T. Fermann, B.J. Mintz, L.A. Burns, J.J. Wilke, M.L. Abrams, N.J. Russ, M.L. Leininger, C.L. Janssen, E.T. Seidl, W.D. Allen, H.F. Schaefer, R.A. King, E.F. Valeev, C.D. Sherrill, T.D. Crawford, WIREs: Comput. Mol. Sci. 2 (2012) 556–565.
[96] M.W. Schmidt, K.K. Baldridge, J.A. Boatz, S.T. Elbert, M.S. Gordon, J.H. Jensen, S. Koseki, N. Matsunaga, K.A. Nguyen, S.J. Su, T.L. Windus, M. Dupuis, J.A. Montgomery, J. Comput. Chem. 14 (1993) 1347–1363.
[97] S.J. Grabowski, Struct. Chem. 28 (2017) 1163–1171.
[98] J.Y. Bae, Y.I. Park, J. Ko, K.I. Park, S.I. Cho, S.O. Kang, Inorg. Chim. Acta. 289 (1999) 141–148.
[99] T. Clark, M. Hennemann, J. Murray, P. Politzer, J. Mol. Model. 13 (2007) 291–296.
[100] P. Politzer, J. Murray, M. Concha, J. Mol. Model. 13 (2007) 643–650.
[101] K. Ruedenberg, Rev. Mod. Phys. 34 (1962) 326–352.
[102] K. Ruedenberg, in: O. Chalvet, R. Daudel, S. Diner, J.P. Malrieu (Eds.), Localization and Delocalization in Quantum Chemistry, vol. I, D. Reidel Publishing Company, Dordrecht-Holland, Netherlands, 1975, pp. 223–245.
[103] R. Núñez, P. Farràs, F. Teixidor, C. Viñas, R. Sillanpää, R. Kivekäs, Angew. Chem. Int. Ed. 45 (2006) 1270–1272.
[104] F. Teixidor, R. Núñez, C. Viñas, R. Sillanpää, R. Kivekäs, Angew. Chem. Int. Ed. 39 (2000) 4290–4292.
[105] F. Teixidor, G. Barberà, A. Vaca, R. Kivekäs, R. Sillanpää, J. Oliva, C. Viñas, J. Am. Chem. Soc. 127 (2005) 10158–10159.
[106] A.M. Spokoyny, C.W. Machan, D.J. Clingerman, M.S. Rosen, M.J. Wiester, R.D. Kennedy, C.L. Stern, A.A. Sarjeant, C.A. Mirkin, Nat. Chem. 3 (2011) 590–596.
[107] J. Grunenberg, Chem. Eur J. 22 (2016) 18678–18681.
[108] J. Fanfrlík, A. Pecina, J. Řezáč, R. Sedlak, D. Hnyk, M. Lepšík, P. Hobza, Phys. Chem. Chem. Phys. 19 (2017) 18194–18200.
[109] B. Wang, S.L. Li, D.G. Truhlar, J. Chem. Theor. Comput. 10 (2014) 5640–5650.
[110] J.A. Nilsson, A. Lyubartsev, L.A. Eriksson, A. Laaksonen, Mol. Phys. 99 (2001) 1795–1804.
[111] T. Lu, F.W. Chen, J. Theor. Comput. Chem. 11 (2012) 163–184.
[112] W. Zou, D. Nori-Shargh, J.E. Boggs, J. Phys. Chem. A 117 (2013) 207–212. Erratum: 120(2016) 2057–2057.
[113] S.A. Cooke, M.C.L. Gerry, J. Am. Chem. Soc. 126 (2004) 17000–17008.
[114] M. Lein, J. Frunzke, G. Frenking, in: D.M.P. Mingos, T. Schönherr (Eds.), Optical Spectra and Chemical Bonding in Inorganic Compounds, Springer, Berlin, 2004, pp. 181–191.
[115] D. Danovich, S. Shaik, F. Neese, J. Echeverría, G. Aullón, S. Alvarez, J. Chem. Theor. Comput. 9 (2013) 1977–1991.
[116] W.B. Schneider, G. Bistoni, M. Sparta, M. Saitow, C. Riplinger, A.A. Auer, F. Neese, J. Chem. Theor. Comput. 12 (2016) 4778–4792.
[117] J.J. Novoa, F. Mota, Chem. Phys. Lett. 318 (2000) 345–354.
[118] S.J. Grabowski, P. Lipkowski, J. Phys. Chem. A 115 (2011) 4765–4773.
[119] G.R. Desiraju, Acc. Chem. Res. 35 (2002) 565–573.
[120] E.R. Johnson, S. Keinan, P. Mori-Sánchez, J. Contreras-García, A.J. Cohen, W. Yang, J. Am. Chem. Soc. 132 (2010) 6498–6506.
[121] C. Viñas, R. Nuñez, F. Teixidor, R. Kivekäs, R. Sillanpää, Organometallics 15 (1996) 3850–3858.
[122] F. Teixidor, R. Núñez, M.A. Flores, A. Demonceau, C. Viñas, J. Organomet. Chem. 614–615 (2000) 48–56.
[123] F. Teixidor, J.A. Ayllón, C. Viñas, R. Kivekäs, R. Sillanpää, J. Casabó, J. Chem. Soc. Chem. Commun. (1992) 1281–1282.